博士論文

Study on metal-organic frameworks (MOFs) deposition onto cellulosic materials (セルロース系材料への金属－有機構造体(MOF)の堆積に関する研究)

李　志強

Li　Zhiqiang

Study on metal-organic frameworks (MOFs) deposition onto cellulosic materials

LI Zhiqiang

Department of Biomaterials Sciences

Graduate School of Agricultural and Life Sciences

The University of Tokyo

Contents

List of Figures

List of Tables

List of Abbreviation

Abbreviation	Definition
MOFs	Metal-organic frameworks
POM	Polyoxometalates
PSM	Post-synthesis modification
TEMPO	(2,2,6,6-Tetramethylpiperidin-1-yl)oxyl
DMF	Dimethylformamide
HYP	High yield pulp
TMP	thermo-mechanical pulp
CHFs	Carboxymethylated high yield pulp fibers
PBS	Phosphate-buffered saline
UV	Ultraviolet
DI	Deionized
FESEM	Field emission scanning electron microscopy
EDS	Energy-dispersive X-ray spectroscopy
ATR FT-IR	Attenuated total reflection Fourier-transform infrared spectroscopy
XRD	X-ray diffractometer
BET	Brunauer–Emmett–Teller theory
H_3BTC	1,3,5-benzene-tricarboxylic acid
EtOH	Ethanol

MeOH	Methanol
NaOH	Sodium hydroxide
CMP	Carboxymethylated filter paper
LbL-org	Layer-by-Layer-organic
LbL-wtr-org	Layer-by-Layer-water-organic

Chapter 1

General Introduction

1.1 Background of metal-organic frameworks

Metal-organic frameworks, namely MOFs, have received remarkable attention in recent years. These crystalline materials are composed of transition metal ions or clusters and organic unites, which are linked by coordinate bonds and can also be named coordination polymers [1, 2]. Due to the reticular synthesis, a three-dimensional porous network with large internal pore volume can be yield. MOFs have the characteristics of well-defined pore structure, large surface area, and structural flexibility, which are in excess of commercial porous materials, such as zeolites or active carbons [3]. These characteristics make the interior structure of MOFs can be chemically varied, with broad application prospects in gas adsorption and separation [4], storage [5], catalysis [6], and many other fields [7-9].

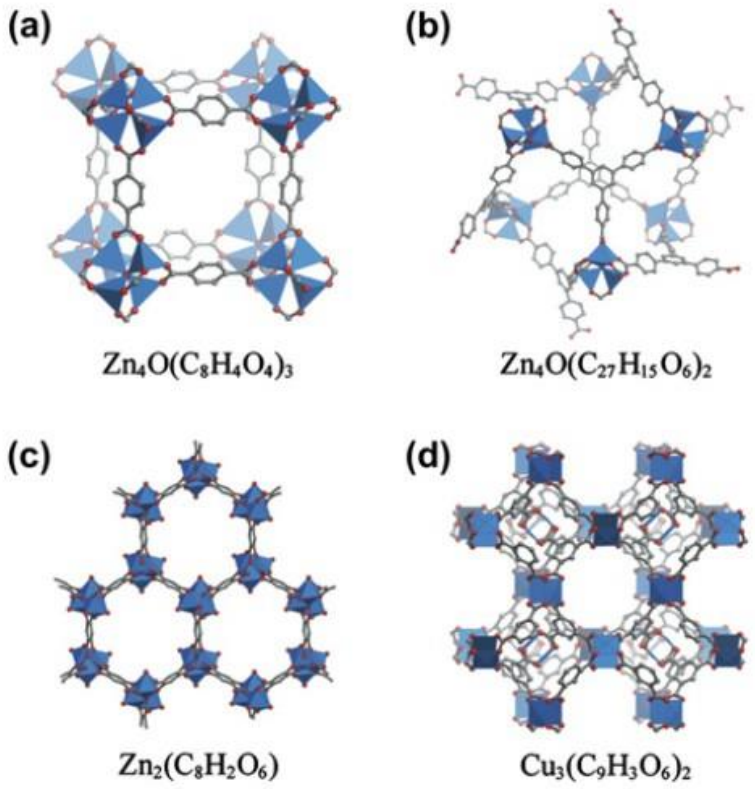

Fig. 1-1 Schematic of typical metal-organic frameworks: (a) MOF-5, (b) MOF-177, (c) MOF-74, (d) MOF-199. [10]

The typical porosity of crystalline metal-organic frameworks structures can be greater than 50% of the MOF crystal volume, which can be formed by organic units (normally are ditopic or polytopic carboxylates and other similar negatively charged molecules) linked to metal-containing units. By altering different kinds of metal-containing units and organic units, MOFs with multifunction and various pore size can be achieved, surface area values ranging from 1000 to 10,000 m^2/g [7]. Fig. 1-1 shows the schematic of four typical metal-organic frameworks with different structures and pore sizes, which are synthesized by different metal units and organic units, Zn_4O and 1,4-benzodicarboxylate of MOF-5, Zn_4O and 1,3,5-benzenetribenzoate of MOF-177,

Zn^{2+} and 2,5-Dihydroxyterephtalic of MOF-74, and Cu^{2+} and 1,3,5-Benzenetricarboxylic of MOF-199.

1.2 Synthesis method of MOFs

In general, metal-organic frameworks are crystallized from a special solution. Pores together with unreacted chemicals of the initial compounds are filled by water and especially organic solvents [11]. Thus, MOFs are conventional synthesized by the routes of hydrothermal or solvothermal, which are normally conducted via electric heating without any other concurrent reactions [12]. From this point of view, the reaction temperature is one of the most important parameters in the synthesis of MOFs [13].

The energy that MOFs synthesis need is usually inputted via the form of conventional electric heating, for instance, a hot source transfers the heating via convection in an oven [13]. However, this kind of method is time-consuming (from several hours to days), alternative energy introduced methods for synthesizing MOFs are developed, such as means of microwave-assisted, sonochemical, electrochemical, and mechanochemical. Diverse energy will result in different duration time, pressure, and energy per molecule in the reaction system [14], which can have a significant effect on the product forming process and end properties. Fig. 1-2 summarizes the synthesis

methods, reaction temperature, and final products in the MOFs preparation.

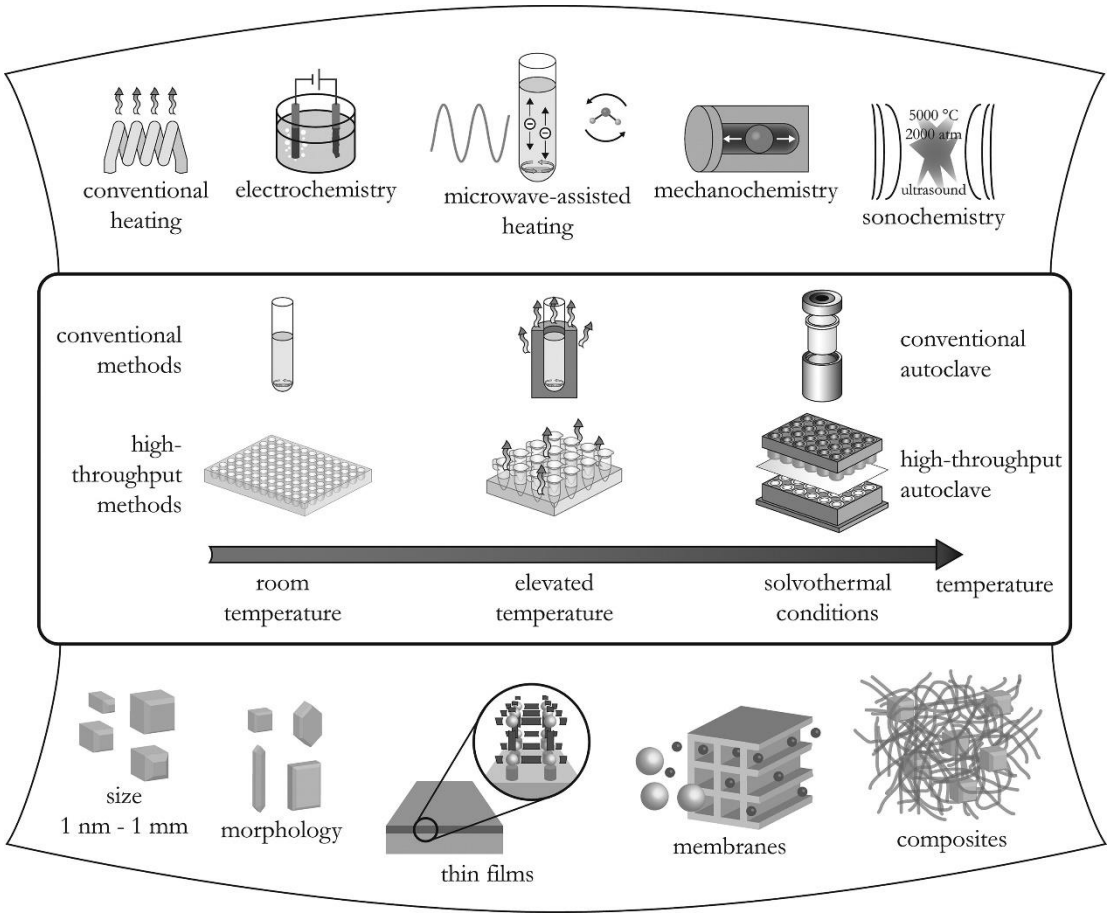

Fig. 1-2 Outline of MOFs synthesis in terms of methods, reaction temperature, and products [13]

1.2.1 Traditional synthesis

The traditional synthesis is usually applied to prepare metal-organic frameworks, which can be categorized into solvothermal and non-solvothermal methods. The term solvothermal refers to reactions occurring in the closed vessels under autogenous pressure above the boiling point of the solvents. Organic solvents are more generally used in solvothermal method than hydrothermal using water as the solvent. Non-

solvothermal reactions occur at the temperature of less than or equal to boiling point under atmospheric pressure, which greatly simplifies the requirement of equipment [11, 13].

Solvothermal synthesis can achieve higher yields and better crystallinity of the final products. Due to the condition of a sealed vessels, the pressure will be promoted, which further increases the heating temperature of solvents (over boiling point) and enhances the solubility of the salts, and finally facilitates the reactions. A typical MOF-5 was synthesized by Yaghi et al. using this method [15]. MOF-5 is a chemical formula of $Zn_4O(BDC)_3$, which is consisted of octahedral Zn_4O linked by ditopic linear BDC. By using triethylamine as the catalyst, H_2BDC and zinc nitrate was dissolved in a solution of DMF/chlorobenzene, leading to deprotonation of H_2BDC and reacted with Zn^{2+} ions. A higher yield procedure has been developed by using DEF as the solvent heated at 105 ºC in a sealed container for MOF-5 crystallization [16]. For non-solvothermal synthesis, some representative MOFs have been synthesized at room temperature by just blending the required chemicals in selected solvents, such as MOF-5, MOF-74, MOF-177, MOF-199, and IRMOF-0[10].

1.2.2 Microwave-assisted synthesis

In the chemistry of synthetic, using the energy of microwave irradiation is a recognized route [17]. Microwave-assisted synthesis depends on electromagnetic waves interacted with moving electric charges. The microwave-assisted heating shows a very energy-saving way of heating contributed by the solution interacting with reactants

directly. This method has the advantages of rapid crystallization, phase selectivity [18], narrow particle size distribution [19], and simple morphology control [20]. Generally, for microwave synthesis, a sealed Teflon container of the mixture of chemicals and suitable solvents is placed in a microwave device and heated at a set temperature for an appropriate time.

Jhung, S.H. et al. [21] first synthesized a kind of MOFs, Cr-MIL-100, using microwave-assisted method. They synthesized the MOF at 220 ºC for 4 h and obtained a yield of 44%, the condition has some degree of comparability of conventional hydrothermal synthesis with a condition of 220 ºC and 4 days. A typical MOF-5 was also synthesized by this method, to reduce the preparation time, a strategy of increasing microwave irradiation time, powder level, and chemicals concentration was applied, but resulted in a reduction of crystal quality [22].

1.2.3 Electrochemical synthesis

The main feature of electrochemical synthesis of MOFs is that the metal ions are continuously supplied from the anodic dissolution int the electrolyte containing dissolved linker molecules rather than metal salts, which will avoid the use of protic solvents, but hydrogen is generated in the process [9]. By using this way, the anions of metal salts, for instance nitrate, perchlorate, or chloride can be excluded during the syntheses, which will be a problem for large-scale production processes. The electrochemical strategy affords the possibility of running a continuous process for achieving a higher MOFs content compared to normal batch reactions [13].

Researchers from BASF first reported the electrochemical synthesis of HKUST-1[13]. In their study, a copper plate was used as the anode immersed in H_3BTC dissolved in methanol with copper cathodes. After 150 min reaction at the applied voltage and currency, a green-blue precipitate was formed. Since then, many other MOFs, such as ZIF-8, Al-MIL-100, Al-MIL-53, and Al-MIL-53-NH_2 were synthesized by using electrochemical strategy with different anodic dissolutions [23].

1.2.4 Mechanochemical synthesis

Mechanochemical synthesis refers that the intramolecular bonds can be broken by introducing mechanical force and then a chemical transformation takes place. Pichon, A., et al. [24] first reported synthesis of porous MOFs by using mechanochemical method. In this study, copper acetate and isonicotinic acid were mixed in a ball mill for several minutes, then $Cu(INA)_2$ MOF was formed. During the synthesis, both the reaction products, water and acetic acid in the MOF pores can be moved by heating. Several typical studies about synthesizing MOFs via mechanochemical method were summarized by Tomislav Friščić [25].

Avoiding organic solvents is the most important advantage of mechanochemical method, because the mechanochemical react can be conducted at room temperature under solvent-free conditions [26]. In addition, using this method can yield quantitative products in short reaction time, usually in 10-60 min. Moreover, in several cases, the metal salts can be replaced by metal oxides as the raw material, which only has the side product of water [13].

1.2.5 Sonochemical synthesis

Sonochemical synthesis refers that chemical reactions occur when applying high energy ultrasound to the reaction mixture. Ultrasound is a periodic mechanical vibration with frequency between 20 kHz and 10 kHz. Since the wavelength of ultrasound is much larger than molecular size, the ultrasound direct interaction between ultrasound and molecules is unlikely to cause chemical reactions. When high-energy ultrasound interacts with liquids, a cycle of alternating compression (high pressure) and rarefaction (low pressure) will be formed. During this process, a phenomenon of cavitation take place, the cavity begins from forming a nucleus, then increases to a limited size, and finally collapses [11, 13]. The ultrasonication will result in the increase of reagents blending and dispersion of particle aggregates, which leads to enhancement of chemicals contacting area. Meanwhile, the dissolution of initial chemicals will also be improved.

A kind of MOF named $Zn_3(BTC)_2$ was first synthesized by sonochemical method in 2008 [27]. In this study, zinc acetate and H_3BTC together with 20% ethanol were treated by sonication for different time (up to 90 min), but even treated for 5 min, a fairly high product yield of 75.3% was obtained. Synthesis of HKUST-1 MOF in DMF/EtOH/H_2O solvent by sonochemical method was also reported [28]. A size of 10-40 nm nanocrystalline powder was achieved after 5 min sonication treatment. Larger crystals (50-200 nm) and higher yields were obtained when raising the treatment time, but a partial decomposition of crystals also occurred. The objective of sonochemical synthesis in MOF preparation is to looking for a method that can be easily implemented

with the features of fast, energy-saving, environmentally friendly and room temperature adaptable, which will be a promising strategy for future scaleup application.

1.3 Performance and application of MOFs

Metal-organic frameworks are a new type of molecular sieve-like coordination polymers, which consist of organic and inorganic compounds, bonded by coordinate bonds. Compared with organic carbon or inorganic molecular sieves and silica, MOFs have the obvious advantage of modifiability, such as obtaining new structure by adjusting the metal ion cluster or organic ligands and post modification by related reactions. In terms of raw material source, the organic linkers include carboxylic acid, sulfonic acid, imidazole, pyridine, and their derivatives, the metal ions or clusters include almost all transition metals and some alkali metals. As for molecular structure, currently synthesized MOFs all have micropore or mesoporous structure and wide chemical applicability. Therefore, MOFs are widely used in the fields of adsorption, separation, antibacterial, photochromism, fluorescence, catalysis, and magnetism.

1.3.1 Gas adsorption and separation

The fundamental principal of selective gas adsorption and separation is based on two parts, one is the adsorbate-surface interactions, which includes the chemical or/and physical interaction between adsorbent and the adsorbate; the other one is the size-exclusion (molecular sieving effect), which is up to the shape and size of selected MOFs. These two impacts can work independently, and also cooperatively [29].

Ma S et al. [30] developed a MOF, PCN-13 ($Zn_4O(H_2O)_3(C_{16}H_8O_4)_3 \cdot 2DMF$), which

involved a pore volume of 0.3 cm^3/g and a square hydrophobic channel of 3.5 Å × 3.5 Å. This MOF was used for separating N_2 for O_2, because N_2 has a larger molecule size of 3.64 Å while O_2 has a smaller molecule size of 3.46 Å. Hence, O_2 can pass through the pore while totally preventing the N_2. Another study concerning gas separation of CO_2 and CH_4 by using amino-functionalized Mil-53 MOF was also reported [31]. The CO_2 molecule has a high affinity for amino groups due to the quadrupole moment, and the experiments showed that CH_4 could pass through the MOF while CO_2 was adsorbed. Therefore, these two gases can be separated at atmospheric condition.

1.3.2 Catalysis

MOFs as a sort of porous material with ultra-high surface area, can be used in catalysis field. In theory, by optimizing the design of pore parameters, MOFs can be applied in each specific catalytic system. In addition, owing to the high content of metal and high crystallinity, each active site is diverse. Hence, in the reported MOFs that can be applied for catalysis, the catalytic activity is mainly determined by the porosity and the specific transition metal center with catalytic activity.

The MOF, HKUST-1 was reported to play the role of Lewis acid catalysts, because it exhibits open metal sites when the solvent removed from the MOF [32]. Schröder et al. [33] reported a functional MOF-5 doped with Ru nanoparticles, and used for alcohol oxidation as a catalyst. But the water sensitive feature of MOF-5 limited its catalytic application. The distinctive catalytic features of MOFs can be developed via investigating the metal centers, organic linkers, particle size, as well as integration of

these.

1.3.3 H_2 and CH_4 storage

Many studies have been conducted to increase store fuel gases such as hydrogen and methane under actual conditions. A container filling porous adsorbent makes the gas can be stored at a much lower pressure, which brings the safe and economic benefits. MOFs can act as such kind of adsorbents due to the characteristics of adjustable pore size and flexible frameworks.

MOF-5 was the first reported study for H_2 storage [34]. Since then, many MOFs have been studied to enhance the hydrogen storage capacity [35]. The hydrogen storage of MOFs is based on physical adsorption, and as we all know, in this mode, the saturated hydrogen adsorption at 77 K is positively correlated with the surface area of the adsorbent. So, rising the surface area will contribute to improvement of hydrogen storage. MOFs have higher surface area than other materials, which attract much attention in this field. Natural gas (mainly methane) is another alternative fuel source. $CuSiF_6(BPy)_2$ was the first reported MOF studied for storing CH_4 gas [36]. Same as hydrogen adsorption, the total weight of methane adsorption is usually increased with enhancing the pore volume of MOFs.

1.3.4 Drug storage and delivery

Generally, different drug delivery strategies can be divided in organic systems and inorganic systems. The former has the advantages of wide range of biocompatibility and the ability to adsorb multiple drugs, but lack a controllable release mechanism

while the latter has a well-organized porous network that can deliver adsorbed drugs at a controlled rate, but with reduced loading capacity [37, 38]. Due to MOFs with adjustable functional groups and tunable pore size consist of organic and inorganic compounds, two parts of the benefits from organic and inorganic materials can be realized.

Two kinds of MOFs, MIL-100 and MIL-101 were found to be applicable for drug delivery because of their well-organized porosity [39]. Due to the different pore size and particle shape of MIL-100 and MIL-101, 1 g dehydrated MIL-100 was reported to uptake 0.35 g ibuprofen while same amount of MIL-101 could uptake 1.4 g ibuprofen. A flexible MOF, MIL-53, having the ability of respiration that can expand its structure after heating, was also developed for drug delivery [40, 41]. It was found to uptake about 20 wt% of ibuprofens with a whole delivery using about three weeks, contributed by full expansion at a high temperature with large pore volume of the MOF.

1.3.5 Antibacterial

The antibacterial ability of MOFs comes from the release of metal, which is in the form of cation or small parts of MOF framework [42]. Such metal can be Ag^{+}, Zn^{2+}, Cu^{2+}, Ni^{2+} that have antibacterial properties, the high porosity of MOFs can ensure the gradual release of metal ions during diffusion or biodegradation process, thereby providing long-lasting antibacterial effect. This process resulted in a continuous antibacterial effect and high durability while restraining the agglomeration and oxidation [42].

Cu-BTC, also named as MOF-199 or HKUST-1, is one of the most famous Cu-

based MOFs, containing Cu(II) as the inorganic part and H_3BTC acid as the organic ligand. It was reported to have strong antifungal property against *Saccharomyces cerevisiae* and *Geotrichum candidum*. And even after 24 hours of microbiological test in a liquid medium, the inhibition zone of Cu-BTC was observed, showing the gradual degradation of MOF structure and slow release of Cu^{2+} ions that related to antifungal effect [43]. Another study reported the antibacterial property of two cobalt-imidazolates, ZIF-67 and Co-SIM-1, and compared to one silver-based MOF, AgTAZ [44]. The results showed that two Co-based MOFs had much higher inhibition zone (about 15 mm) against selected fungus than that of AgTAZ (about 2 mm). The Co^{2+} ions were found to diffuse into the agar medium, which played an antibacterial effect. Even after 3 months, the antibacterial activity was still high and almost unchanged, showing the MOFs have excellent durable antibacterial properties and extended release of antibacterial agents.

1.3.6 Other applications

Due to the characteristic advantages of both organic and inorganic porous materials, metal-organic frameworks have also been developed in many other specific applications. Such as magnetic properties, luminescence and sensors, photochromic properties, etc. [29] Many other new potential applications of MOFs need to be developed based on specific utilization.

1.4 MOF composites

Diverse metal-organic frameworks synthesized by existing strategies have many excellent properties as mentioned above, but the synthesized MOFs are general

insoluble in water and organic solvents, and with very small size, form of powder, and poor processability, which limit the applications of MOFs in many aspects [45, 46]. Therefore, industrialized utilization and expanding the application fields have become an increasingly concerned issue for researchers. Much attention has been focused on preparation of MOFs modified functional materials with MOFs as a matrix or MOFs as an enhancement for composites. Using MOFs to modify or compound other materials can not only maintain the existing performance of MOFs, but also further improve the properties of composites. Varieties of substrates with different properties were reported for MOFs deposition, such as silicon, alumina, TiO_2, ceramics, carbon nanotubes, glass, metals, fibers, etc.

1.4.1 Preparation of MOF composite

Various methods are performed to fabricate MOF-based composites. These methods can be divided into several types, direct growth, layer-by-layer growth, secondary growth, and chemical solution deposition.

(1) Direct growth

Direct growth method also known as in situ growth method, which is generally performed by immersing the selected supports in the reaction solutions involving the metal salts and ligands for MOFs synthesis. The nucleation sites on the carrier can be produced by microwave-assisted heating, thereby allowing crystals to grow on the substrate with a thickness of several microns. The support can also be immersed in the preheated reaction mixture where nucleation occurs and then crystallization process.

Due to the heterogeneous nucleation, these two methods can hardly achieve continuous thin film on the substrates. Hence, to obtain high quality films, modifications of the substrates are needed [13].

Direct growth method can be applied for preparing MOFs modified functional materials. Liu et al. [47] reported a study concerning this method, they immersed porous α-Al_2O_3 substrate in the terephthalic acid dissolved in DMF for a period of time, then adding zinc nitrate hexahydrate, reacted at 105 ºC in a reactor. The thickness of MOF-5 layer of the composite was about 5 μm. But the orientation was unclear and easy to fall off. Generally, MOFs grow more easily in solution, so when introducing the substrate, the growth status of the MOFs is related to the nature of substrate. Therefore, to improve the growth state of MOFs on the substrate, the substrates needs to be functionalized. Usually, the substrates are modified to expose more active groups (such as hydroxyl, carboxyl, and amino) that can be easily reacted with organic ligands of MOFs. Huang et al. [48] reported a modified strategy, they used 3-aminopropyltriethoxysilane to aminate the α-Al_2O_3 substrate and grow a dense and continuous ZIF-90 crystal layer on the surface by in-situ growth method. The mechanism of ZIF-90 modified α-Al_2O_3 material was that during the amination treatment of the substrate, 3-aminopropyltriethoxysilane reacted with the surface of α-Al_2O_3 material, providing a site for the growth of MOFs. Then, the organic ligands of ZIF-90 reacted with the growth sites of the aminated substrate to obtain dense MOFs modified α-Al_2O_3 functional materials.

(2) Layer-by-layer growth

In order to obtain homogeneous, controllable orientation and thickness of MOFs films on the selected substrates, layer-by-layer (LbL) method for growth of MOFs is developed. In LbL growth method, the substrate is first immersed in the solution of metal salts, then washed by suitable solvent to remove unreacted chemicals, and immersed in the solution of organic ligands for MOFs growth, finally rinsed as one growth layer and repeated the growth cycle. Although layer-by-layer method has many advantages compared to direct growth, some drawbacks should be noticed. The substrate normally needs to be modified, and due to the repeating cycles of immersion and rising, the LbL method is time-consuming [49].

Shekhah et al. [50] first used layer-by-lay method to grow HKUST-1 MOF onto Au substrate. The Au surface was functionalized by COOH, then the substrate was successively immersed in Cu^{2+} and H_3BTC solution, and repeating the process to obtain HKUSU-1@Au composite with increasing thickness of MOF films.

(3) Secondary growth

Secondary growth, namely seeded growth, is generally conducted by coating the substrate with a seed layer (spin or dip coating), then the seeded substrates are immersed in reaction solution containing metal salts and organic linker for MOFs growth. The subsequent growth method is like direct growth method, usually performed in a solvothermal system. Secondary growth method is able to get a controllable MOF thickness and orientation compared to direct growth, so this method is often used for preparing membranes [13].

ZIF-7 was reported to growth on α-alumina support by seeding growth method [51].

Prior to synthesize ZIF-7, the α-alumina was dip-coated with as-synthesized crystals as the seeded layer with PEI added as the dispersions. PEI in the reaction solution could improve the attachment between seeds and support by H-bonding. Then the ZIF-7 was grown based on the seeded layer in the form of continuous and oriented membranes.

The direct growth usually results in loose MOFs crystals on the selected substrate, but this procedure can be used to conduct a seed layer for secondary growth. That is, employing a MOF on the substrate prepared by direct growth method as the seed layer, then the subsequent MOFs can grow on the MOF seed layer. The seed layer can be the target MOF for composite preparation or other MOFs. Gascon et al. [52] used Cu-BTC as the seed layer, which was spin-coated on the porous Al_2O_3 substrate, then HKUST-1 crystals were secondary grown on the seeded layer.

(4) Chemical solution deposition

The term chemical solution deposition is that the presynthesized MOFs nanocrystals were deposited on the substrate by spin- or dip-coating procedure in a suspension. This strategy is able to prepare thin films via dispersions of MOFs crystals. The film thickness can be adjusted by several depositions. This route is also applied in industry due to the features of low-cost and large-scale practicability.

It was reported that silicon wafers were dip-coated with colloidal dispersion of ZIF-8 crystals to form a ZIF-8 film [53]. The density and thickness of the film could be adjusted by changing the taking speed and particles concentration.

1.4.2 MOFs functionalized composites

(1) MOFs@metallic oxide

Metallic oxide materials with controllable shape, size, crystallinity, and function, are widely applied in electronics, optics, catalysis, solar energy collection, electrochemical energy, etc. To further improve the performance of metallic oxide and introduce new functions, many studies have been conducted to integrate metallic oxides, especially those with magnetic or semiconductor properties and MOFs into core-shell structure [54].

Lohe et al. [55] recently reported iron oxide particles grafted with organic ligand carboxylate groups as seed for MOF growth. The magnetic functionalization of aluminum-based and copper-based MOFs by superparamagnetic γ-Fe2O3 was studied. Results showed that the superparamagnetic functionalization can enable the MOFs catalyst to be quickly separated from the reaction medium, and realized the possibility of the release of controllable drug ibuprofen caused by magnetic induction heating of the magnetic composite material.

(2) MOFs@Polyoxometalate

Polyoxometalates (POM), a kind of inorganic molecular compounds, are composed of discrete anionic metal-oxygen clusters with diversity in size and shape. POM is widely applied in catalysis, pharmaceuticals, electrochemistry, photochromism, magnetism, etc. POM has attracted much attention especially in the field of catalytic chemistry. But its small specific surface area and poor stability limits its application [56]. By fixing POM in porous materials can improve the stability of POM and optimize its

catalytic performance. Compared with traditional porous materials, porous MOFs have the obvious advantages of large specific surface area and high porosity. Therefore, synthesis of MOFs@POM composite is expected to improve the dispersion of POM in MOFs to prevent the aggregation and deactivation of POM, and enhance the catalytic performance.

Maskimchuk et al. [57, 58] reported a MIL-1012@POM composite obtained by immersion route by using MIL-101 as the main body, which showed good catalytic selective activity for the oxidation reaction. However, issues including low POM loading, poor uniformity of composite materials and leaching of guest POM during impregnation still need to be considered. Based on template effect of POM, Kuang et al. [59] used POM as a non-coordinating anionic template to construct three-dimensional MOFs. MOFs@POM composites are usually formed by self-assembly method under hydrothermal conditions. The composite prepared the synthesis method has the advantage that POM is easily encapsulated in MOFs, and the limiting effect of MOF pores makes the POM difficult to leach out, thereby avoiding the aggregation and deactivation of active substances.

(3) MOFs@organic-polymer

Organic polymers have unique properties such as convenient production, light weight, excellent thermal stability, and chemical resistance. They are easy to integrate with other functional materials to prepare composites. Therefore, it is necessary to establish a new synthetic mechanism to control the doping or growth of porous MOFs in polymers. A series of composites constructed by MOFs and organic polymers in

various combinations have both two properties.

The research of polymer filling in crystalline porous bodies with tunable nanochannel structure has been widely concerned. Uemura et al. [60] pioneered the use of porous MOFs with various sizes, shapes, dimensions, and surface functions as closed polymerization nanoreactors, especially the active sites on the pore surface of MOFs can be used a nano model for polymer synthesis and catalyst. Lee et al. [61] prepared the ZIF-8@polystyrene microspheres with core-shell structure under solvothermal conditions using the conjugation effect between porous MOFs and organic polymers, and the thickness of ZIF-8 layer could be controlled by the number of growth cycles. Considering that template synthesis is a common strategy for preparing layered hollow microspheres, especially for the holes in the shell, the composite was etched using DMF to remove the polystyrene core layer, forming a unique ZIF-8 layer with hollow structure. This method provided an important way for preparation of MOFs with hollow structure.

(4) MOFs@MOFs

MOFs@MOFs core-shell structure functional materials can not only improve the porous properties of single MOF, but also add new functions without changing the core or shell MOFs single crystal body characteristics. To contracture a multi-functional core-shell structure MOFs@MOFs, there are two main synthesis strategies: a) One MOF is used as a seed layer, and the other MOF are epitaxially grown on the surface of the seed layer to form shell MOF. The composite has two different metal centers and form different crystalline regions in the two-shape MOFs separation area. The key of

method is the close lattice matching between the core MOF and the shell MOF [62]. b) Post-synthesis modification (PSM), including the controlled exchange between residual number of organic ligands and metal framework ions, and the selective reaction of ligands. The post-modification of the metal centers and organic ligands can selectively restrict MOF to each other's shell or core layer.

Based on the epitaxial growth of dissimilar metals, Kon et al. [63] studied the epitaxial growth of two different organic ligands, BDC and BDC-NH_2, to form the core-shell structure MOFs@MOFs. MOF-5 (Zn-BDC) was used as a seed crystal immersed in the precursor solution of IRMOF-3 (ZnBDC-NH_2) to obtain the core-shell structure, and vice versa. Results showed that with the change of the ratio of input amount of two organic ligands, the synthesized composite crystal changed from colorless MOF-5 to orange IRMOF-3, showing high spatial color contrast and no effect on the porosity of MOFs@MOFs, while the specific surface area was between MOF-5 and IRMOF-3.

1.5 Cellulosic materials for MOFs deposition

Many hard substrates for MOF deposition have the disadvantage of high weight, complicated manufacture process, and high cost. Compare with these substrate, cellulosic fiber derived from abundant plant resource have inherent advantages of low specific gravity, low cost, flexibility, recyclability, and biodegradability [64], and also many active chemical groups in the cellulosic materials. Therefore, cellulosic materials can be suitable substrates for MOFs deposition with some special characteristics.

1.5.1 Chemical modification of cellulosic materials

The main content of cellulosic materials is cellulose, which is polysaccharide consisting of a linear chain of hundreds or thousands of D-glucopyranose linked by β-1,4-glycosidic bonds [65]. The hydroxyl groups of cellulose can be subjected to chemical modifications for incorporation of metal-organic frameworks. These modifications of cellulosic substrates can be divided into three: expose more native moieties, organic group modification, and inorganic oxides modification [66].

(1) Expose more native moieties

The native moiety of cellulosic materials that can mimic the complexing moieties of MOFs is hydroxyl groups, especially the hydroxyl group of C6 of cellulose. Therefore, more MOFs can be deposited on the cellulosic substrates if more hydroxyl group can be exposed. This method is the easiest way for MOFs growth modification compared to other two methods.

Several studies have been performed by modifying cellulosic substrates. Ozer et al. [67] used cotton as the substrate for MOFs growth, cotton was simply treated by sodium hydroxide for the purpose of cleaning and more hydroxyl groups explosion. It was also reported in another study that cotton fabric was activated by oxidation with hydrogen peroxide and then the resultant cotton was used for Cu-BTC MOFs deposition [68]. TEMPO oxidation method was also used for cellulosic material pretreatment. Duan et al. [69] treated the delignified corncobs by TEMPO oxidation process of hydroxyl group to carboxyl group, which enhanced the deposition of MOFs on cellulosic materials.

(2) Organic group modification

Cellulosic materials, take the case of cotton, which can be subjected to different surface chemistry modifications, such as esterification, etherification, nitration, acetylation, phosphorylation, and sulfation [70, 71]. Introducing an organic group that can mimics the complexing moieties of the MOFs will result in stronger interaction between the cellulosic substrate and MOFs compared to cellulose native groups.

As one of the earliest reports of cotton functionalization with MOFs, da Silva Pinto et al. modified the cotton substrate by a basic carboxymethylation treatment [72]. The carboxymethylated cotton surface could fix Cu^{2+} by electrostatic interactions and then accelerate the growth of MOF-199. In order to obtain much improvement of carboxymethylation of cotton, another study used chloroacetate and sodium hydroxide in ethanol/water (2:1) solution and the resultant substrate was used for MOFs deposition [73]. Pyromellitic acid was also used for introducing carboxylic groups on the fiber surface through esterification reaction [74]. As well as pure linen and viscose specimens were treated by pre-hydrolyzed 3- glycidyloxypropyltrimethoxysilane and then used for NH_2-MIL-125(Ti) growth [75].

(3) Inorganic modification

In some studies, inorganic oxides integrated onto the fiber surface can also mimic the inorganic part of MOFs. Wang et al modified the cellulose nanocrystals by grafting magnetic Fe_3O_4 and then used for Zn-BTC growth [76]. Yang et al. treated the paper with precipitated calcium carbonate (PCC), then the interfiber bonding by hydroxyl groups reduced, which offered more available hydroxyl groups for complexing MOFs [77].

1.5.2 Cellulosic substrate for MOFs deposition and application

Many cellulosic materials have been developed for construction of MOFs/Cellulosic material composites, from nano scale cellulose to macroscopic fiber, to suit different applications.

(1) Cellulose polymer

Hydroxypropyl cellulose was reported to be used as a raw material for preparing cellulose/MOFs composites [78]. By introducing sulfonic acid functional groups, the modified cellulose showed high proton conductivity. And then integrating the modified cellulose with an aluminum fumarate MOF, which was used as the electrolyte for all-solid-state supercapacitor at low humidity.

Cellulose acetate was also reported to fabricate cellulose/MOFs composites, due to the cellulose acetate is easily electrospun. Several MOFs were used to be loaded on for enhancement of the production of hollow fibers. Such as hybrid UiO-66 for mercaptan removal from natural gas [79], MOF-199/cellulose acetate membranes for catalytic applications in continuous flow process [80], a pearl-necklace-like composite membrane prepared by in situ intergrown ZIF-67 on the 2-methylimidazole/cellulose acetate electrospun nano fibers [81], HKUST-1 and ZIF-8 synthesized within cellulose acetate fibers for CO_2/N_2 adsorption [82].

Bacterial cellulose has also been reported for making composites with MOFs. Au-Duong et al first reported bacterial cellulose as the substrate for making a composite with ZIF-8 [83]. The bacterial cellulose was modified by self-polymerization of polydopamine and then used for ZIF-8/bacterial cellulose composite preparation, which

was applied for iodine capture. M. Ashour et al. [84] used water as the solvent to synthesize MIL-100(Fe)/bacterial cellulose nanocomposites and the products were applied for separating arsenic and Rhodamine B from aqueous solution.

(2) Nanocellulose

Nanocellulose materials show a great promise as effective carriers and supporting substrates. Several studies have been performed by using nanocellulose material for metal-organic frameworks hybrid. Zhu et al. [85] reported a facile method to prepare a flexible and porous aerogel by combining functional MOFs and structural cellulose nano crystals (CNCs) and the resultant aerogels were used for separations applications. Matsumoto and Kitaoka [86] reported a nanocellulose film with nano porous MOFs embedded. In their study, TEMPO oxide cellulose nanofibers (TOCN) with surface carboxylated were used for MOF (ZIF-90) deposition, and the hybrid crystals were filtered on a commercial filter paper. The final products with gas-barrier properties were used for separation of CO_2 from CO_2/CH_4.

Lu et al. [87] reported a cellulose-supported magnetic Fe_3O_4-MOF composite using the cellulose micro-fibrils (CMF) as the basic substrates. The CMF improved the dispersion of MOF crystals and Fe_3O_4 nanoparticles, then the catalytic performance of the resultant composite was enhanced.

(3) Cellulosic fiber

Cellulosic fibers are the main substrates for MOFs deposition in the cellulosic materials because of their easy access and close to industry. In an initial study, pulp fibers were directly used for MOFs growth [88], chemi-thermomechanical pulp (CTMP),

unbleached kraft pulp, and bleached pine kraft pulp. The CTMP fibers had the highest amount of MOF growth compare to other two pulp fibers, the authors attributed this to the high content of carbonyl or carboxylic acid group of CTMP. In another study, da Silva Pinto et al. [72] modified the cotton fiber by a carboxymethylation treatment, which proved that the deposition of MOFs to the carboxylate groups from the anionic cellulose is indeed and that the presence of carboxyl groups plays a stabilizing role for MOFs formation.

Different applications of MOFs/cellulosic fibers composites were developed, such as antibacterial properties [89], catalytic of nitric oxide release [90], luminescent properties [67], removal of ethion insecticide from water [68], etc. of MOFs/cotton fabric.

(4) Paper

Paper, as the most common cellulosic material, is also used to fabricate MOF/paper composite. Two typical routes were used for preparing the composite, a) the MOFs were used as a special filler during the papermaking, b) MOFs were growth on the ready-made paper surface like a kind of coating.

Su et al. [91] reported ZIF-8 functionalized cellulose air filter paper, the cellulose fibers were functionalized by growth of ZIF-8 nanocrystals, then the resultant samples were used to fabricate air filters with gas adsorption ability by freeze-drying technique. Jeehyun Park and Moonhyun Oh [92] constructed a filter paper composite with ZIF-8 and ZIF-67 grown on the paper surface like a coating procedure, which was used for dyes capture from water.

1.6 Objective of this study

Metal-organic frameworks (MOFs), a new class of porous crystalline materials composed of transition metal ions linked by polyfunctional organic linkers with coordination bond, have been drawn much attention over recent years due to their large surface area and adjustable pore size. Due to their excellent properties, MOFs have been widely studied for various applications, such as gas storage, separation, sensing, catalyst and antimicrobials. MOFs normally present as a form of powder, so for industrial application processes, it is essential to mold or form these crystalline powders to certain shapes for a specific use. Cellulosic materials derived from abundant plant resource have inherent advantages of low specific gravity, low cost, recyclability and biodegradability and many active chemical groups on the fiber surface. Therefore, the objective of this work is to study the metal-organic frameworks deposited onto cellulosic materials in term of green synthesis and optimum fabrication routes, by using less organic solvent and improving the depositing efficiency. The research and application of the MOFs functionalized cellulosic materials using the strategy investigated in this work will expand the high-value applications of cellulosic materials with the advantages of being more economical and environmental-friendly.

Chapter 2

Synthesis and characterization of Cu-BTC metal-organic frameworks onto lignocellulosic fibers by layer-by-layer method in aqueous solution

2.1 Introduction

Metal-organic frameworks (MOFs), a new class of porous crystalline materials composed of transition metal ions linked by polyfunctional organic linkers with coordination bond, have been drawn much attention over recent years due to their large surface area and adjustable pore size [7, 13]. Due to their excellent properties, MOFs have been widely studied for various applications, such as gas storage [93], separation [94, 95], sensing [96], catalyst [97, 98] and antimicrobials [99].

MOFs normally present as a form of powder, so for industrial application processes, it is essential to mold or form these crystalline powders to certain shapes for a specific use, such as beads or pellets for gas absolution, catalyst, and energy storage, ensuring a low-pressure drop and high performance [45, 88]. Several studies have already succeeded in depositing selected MOFs on some suitable substrates offering high thermal stability, for example, ceramic beads [100] alumina and silica [101]. But these hard substrates have the disadvantage of high weight, complicated manufacture process, and high cost. Compared with these substrates, lignocellulosic fibers derived from abundant

plant resource have inherent advantages of low specific gravity, low cost, recyclability and biodegradability [64] and many active chemical groups on the fiber surface. Therefore, lignocellulosic fibers and fiber-based material can be suitable substrates for industrial applications of MOFs.

Several pieces of research have been conducted to deposit MOFs onto fiber surface for specific applications. da Silva Pinto et al. [72] studied the mechanism for chemical bonding and growth of Cu-BTC onto cotton substrates, indicating the presence of carboxyl groups in modified fibers plays a stabilizing role in the formation of Cu-BTC crystals. MOFs deposited onto fibers and fiber-based materials surface showed an antibacterial activity [89, 102, 103], applied in purification of waste water by removing dyes [68, 104], separation of certain gas and pollutant [85, 86, 105], removing insecticide [68] and adsorption [77, 106]. All the researches above use pure cellulose material (cotton, bleached fiber, and nanofibrils) as the substrates for growth of MOFs and organic solvents as the reaction solvent, for instance dimethylformamide (DMF), ethanol and methanol, which do not make full use of lignocellulosic fibers and bring difficulties for further treatment of liquid waste.

Recently, using salts as linker sources to synthesize MOFs in the water at room temperature was developed [107], where they used organic salts (instead of their homologous protonated organic ligands) as anionic linker sources to prepare MOFs in aqueous solution at room temperature. In conventional preparation strategies, restricted condition is needed, such as high temperature and pressure and organic solvents. The corrosive acid (CH_3COOH, HNO_3, etc., depending on metal anion source) produced by

reaction reagent will fill the pores of synthesized MOFs, normally adding deacid reagent (such as triethylamine) to reduce this effect. Therefore, application of this synthesizing strategy will have the energic or economic advantages and makes green preparation system, and the needless corrosive acid will be replaced by organic salts (trimesic salts of this study). Drawing inspiration from this work, Zn-BDC metal-organic frameworks deposited on cotton fabric and polyacrylonitrile were studied using terephthalic salts [108, 109]. The color of Zn-BDC is white so it's difficult to identify the Zn-BDC on the fiber surface just by visual observation compared with the blue Cu-BTC. And the MOFs just deposit on the fabric surface, which will achieve a smaller number of MOFs on the substrate compared with pulp fibers. To our best knowledge, no studies of using trimesic salts to synthesize Cu-BTC metal-organic framework crystals onto high yield fibers in aqueous solution at room temperature have been reported. Unlike the solvothermal method of synthesizing MOFs at high temperature and pressure, layer-by-layer growth of MOFs on the fiber surface is an optimum approach to achieve more amount and uniform distribution of MOFs onto fiber substrate [90, 110].

In this study, the composites of Cu-BTC metal-organic framework onto high yield pulp fibers were prepared in aqueous solution using trimesic salts as linker sources for coordination bonding with copper. The lignocellulosic fibers were first subjected to a carboxymethylation process for obtaining carboxyl group, then the Cu-BTC crystals depositing onto fibers were prepared by a layer-by-layer method and the synthesis temperature and time was also investigated. The as-prepared composites were further

characterized by various techniques, such as ATR FT-IR, XRD, SEM, and specific surface area analyzer.

2.2 Experimental Section

2.2.1 Materials

High yield pulp (HYP) fibers used in this study were unbleached, never-dried thermo-mechanical pulp (TMP, mixture of Picea jezoensis and Abies sachalinensis), kindly provided by Nippon Paper Industries Co., Ltd. Copper (II) acetate monohydrate ($Cu(OAc)_2 \cdot H_2O$), 1,3,5-benzene-tricarboxylic acid (H_3BTC), sodium chloroacetate ($ClCH_2COONa$), sodium hydroxide (NaOH) were purchased from FUJIFILM Wako Pure Chemical Corporation, Japan. All chemicals were used as received without any further purification. Lab-made deionized water was used throughout all the experiments.

2.2.2 Carboxymethylation of high yield pulp fibers

High yield pulp fibers mainly consist of lignin and cellulose with a small amount of hemicellulose, and the phenolic hydroxyl of lignin and alcohol hydroxyl of cellulose and hemicellulose can be carboxymethylated by sodium chloroacetate with sodium hydroxide as a catalyst [111]. 10 g of fibers were immersed in 250 mL 1 M sodium chloroacetate solution prepared by 15% (w/v) NaOH solution, stirring at 50 ºC for 1h. Then the carboxymethylated high yield pulp fibers (CHFs) were rinsed thoroughly using deionized water to the neutral condition. The carboxyl group content of original and carboxymethylated fibers was determined by the methylene blue method [112-114].

50 mg of fibers were immersed in a mixture of 25 mL of 1mM methylene blue solution and 25 mL PBS buffer solution (pH=8.5), stirring at room temperature for 20 h, then filtered with a glass filter. 2.5 mL of the filtrate was diluted to 50 mL using deionized water. Then the diluted filtrate was measured by UV-visible spectroscopy (UV-1700, Shimadzu, Japan) at a wavelength of 664 nm. The carboxyl group content was calculated by the ratio of the increment of methylene blue between carboxymethylated and original fibers to dry fiber weight.

2.2.3 Preparation of Cu-BTC in aqueous solution

The preparation process of Cu-BTC was revised from [10], the organic solvents and H_3BTC were replaced as water and Na_3BTC respectively. 860 mg (4.31 mmol) of $Cu(OAc)_2 \cdot H_2O$ was dissolved in 12 mL DI water, added a mixture of 500 mg of H_3BTC (2.38 mmol) and corresponding NaOH (285.6 mg, 7.14 mmol) dissolved in 12 mL water, stirring at room temperature for 10 min and allowed to stand for an hour. The product was subjected to centrifugation, removal of supernatant liquid and redispersion with water for three times, and then freeze-dried.

2.2.4 Preparation of Cu-BTC@CHFs composites in aqueous solution

250 mg of CHFs were immersed in 12 mL of $Cu(OAc)_2 \cdot H_2O$ (860 mg, 4.31 mmol) aqueous solution, stirring for 10 min at room temperature, then 12 mL of Na_3BTC aqueous solution (mixture of 500 mg of H_3BTC and 285.6 mg of NaOH) was added, the reaction was performed at different temperatures (R.T., 50 ^oC, and 75 ^oC) and different time (10 min, 4 h, 8 h, 16 h, and 24 h) using a magnetic stirrer. Then the

product was washed thoroughly using water to remove unreacted chemicals and Cu-BTC not deposited on fibers. This one preparation cycle was considered as one growth layer. The Cu-BTC@CHFs composite was prepared by a layer-by-layer method. Another growth layer was conducted based on the former layer of the resultant sample by repeating the process above. The samples were treated with 2, 4 and 6 layers, then freeze dried to obtain final products, as shown in Fig. 2-1.

Due to some fines of fibers may lose during washing, ash content method was used to determine the deposit ratio of Cu-BTC onto fibers. A certain weight of CHFs and Cu-BTC were ignited in a muffle furnace at 900 ºC for 1 h, after complete combustion, samples were cooled slightly and then placed in a desiccator. Samples were weighed when reaching room temperature. The ratio of ash weight and dry sample weight was ash content. The ash weight of Cu-BTC@CHFs was also determined in this way. Then deposit ratio can be calculated by using a binary equation of sample weight and ash weight, as follows in Eq. (1), (2)

$$\begin{cases} x + y = m \\ ax + by = n \end{cases} \tag{1}$$

$$\text{Deposit ratio} = \frac{x}{m} \times 100\% \tag{2}$$

Where, x and y are the weight of Cu-BTC crystal and fiber in Cu-BTC@CHFs, respectively; a and b are ash content of Cu-BTC crystal and fiber, respectively; m and n are the weight of Cu-BTC@CHFs sample and its ash weight, respectively.

2.2.5 Characterization

Field emission scanning electron microscopy (FESEM, S4800, Hitachi, Japan)

with an EDS was used to observe the surface morphologies of samples coated with platinum for 30 s. The IR spectra were performed on a Fourier transform infrared spectrometer with attenuated total reflectance (ATR) mode (Nicolet 6700, Thermo Fisher Scientific Corp, Japan). A total of 128 scans at a resolution of 4 cm^{-1} were performed for each sample. An X-ray diffractometer (XRD, Rigaku Corp) was used to analyze the crystalline phase of each sample from 5° to 40° at 2.5 degrees per min. A current of 40 mA and voltage of 40 kV were used with a Cu (λ=0.15418) standard target. The gas adsorption isotherms of Cu-BTC nanocrystals, Cu-@CHFs were measured by a surface area analyzer (NOVA 4200e, Quantachrome Instrument Corp), using nitrogen gas as the adsorption source at 77 K.

2.3 Results and discussion

2.3.1 Concept of preparation of Cu-BTC@CHFs in aqueous solution

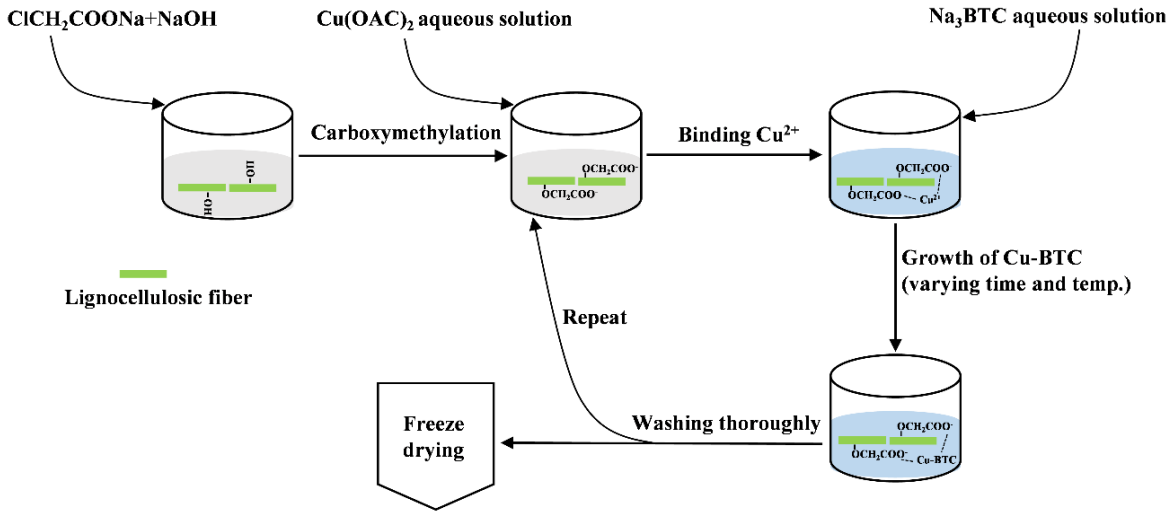

Fig. 2-1 Schematic of the preparation of Cu-BTC@CHFs in aqueous solution

To make full use of the biomaterials and the process more environmentally friendly, we used high yield pulp (HYP) fiber as the substrate for Cu-BTC metal-organic framework growth and water as the solvent. High yield pulp fiber is derived from abundant plant resources and maintains most lignin and cellulose in raw materials, which contain rich alcoholic and phenolic hydroxyl groups, can be a suitable substrate for growth of Cu-BTC metal-organic frameworks. For the preparation of Cu-BTC@CHFs in aqueous solution, we drew inspiration from the study of [107], they used terephthalate salts as the linker source to synthesize several metal-organic frameworks in water. Following this practice, we used sodium trimesic as the linker sources and water as the solvent to prepare the Cu-BTC metal-organic framework.

Fig. 2-1 shows the schematic process of the present study, including carboxymethylation of the fiber, followed by Cu^{2+} ion binding and growth of Cu-BTC. The process, designed to grow Cu-BTC metal-organic framework on the high yield pulp fiber surface, is that the HYP fiber is first subjected to carboxymethylation process so that the carboxylic group can be obtained; successively, the resultant fiber will be utilized for Cu^{2+} binding and then growth of Cu-BTC under different conditions and layer-by-layer method, then freeze dried to get the final products.

2.3.2 Carboxymethylation of high yield pulp fibers

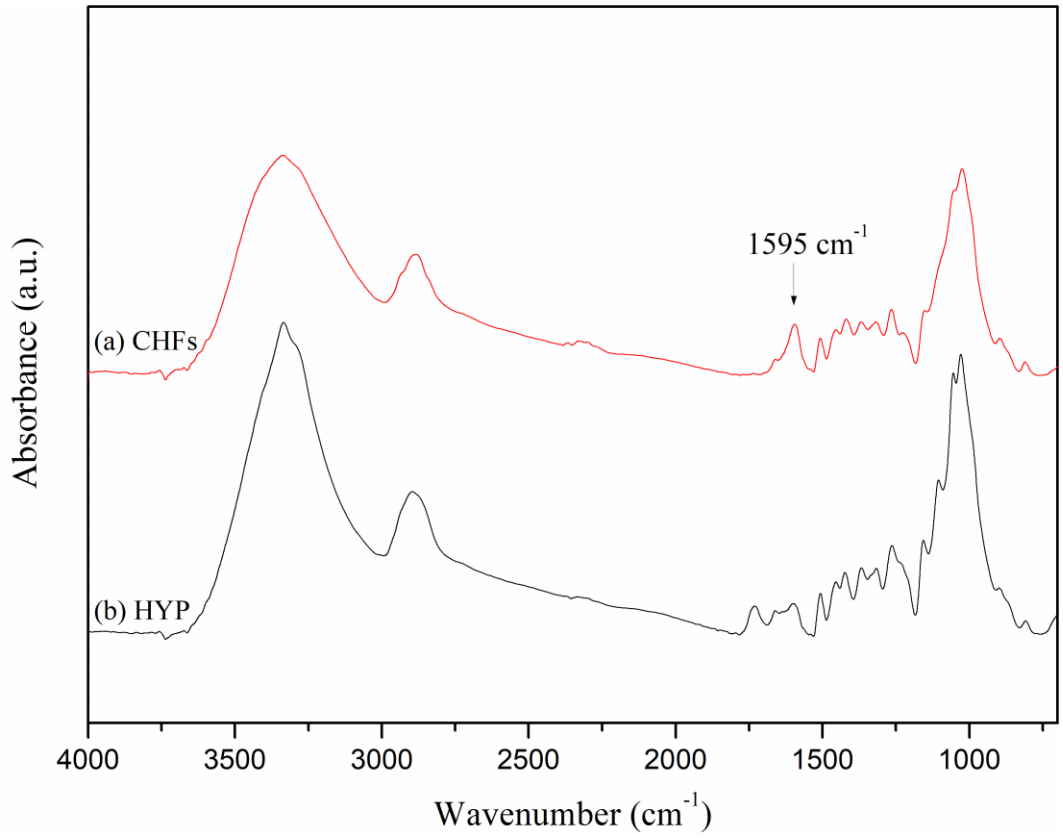

Fig. 2-2 ATR FT-IR spectra of carboxymethylated (a) and original (b) HYP fibers

Table 2-1 Carboxyl content of original and carboxymethylated HYP fibers

Samples	Carboxyl content (mmol/kg)
Original HYP	50 ± 1
CHFs	218 ± 2

In order to achieve the growth and immobilization of Cu-BTC onto HYP fiber, the material was modified by a classical carboxymethylation process. This was implemented by the reaction between lignocellulosic fiber and sodium chloroacetate using sodium hydroxide as a catalyst, as shown in Fig. 2-1.

Carboxymethylation process was monitored by ATR FT-IR shown in Fig. 2-2. The appearance of an absorbance peak at 1595 cm^{-1} for carboxymethylated lignocellulosic fiber indicates the presence of C=O stretching band, which illustrates the formation of carboxymethylated high yield fibers (CHFs). The results are consistent with carboxyl contents of original and carboxymethylated HYP fibers, which increase from 50.08 ± 1.13 mmol/kg to 217.55 ± 2.46 mmol/kg, as shown in Tab. 2-1, the value is higher than a previous report with 34.8 ± 1.3mmol/kg of carboxyl contents of oxidized cotton [68]. Thus, a suitable substrate with the carboxylate group that could bind Cu^{2+} and then facilitates the growth of Cu-BTC is obtained.

2.3.3 ATR FTIR spectra of Cu-BTC@CHFs prepared in different conditions and growth layers

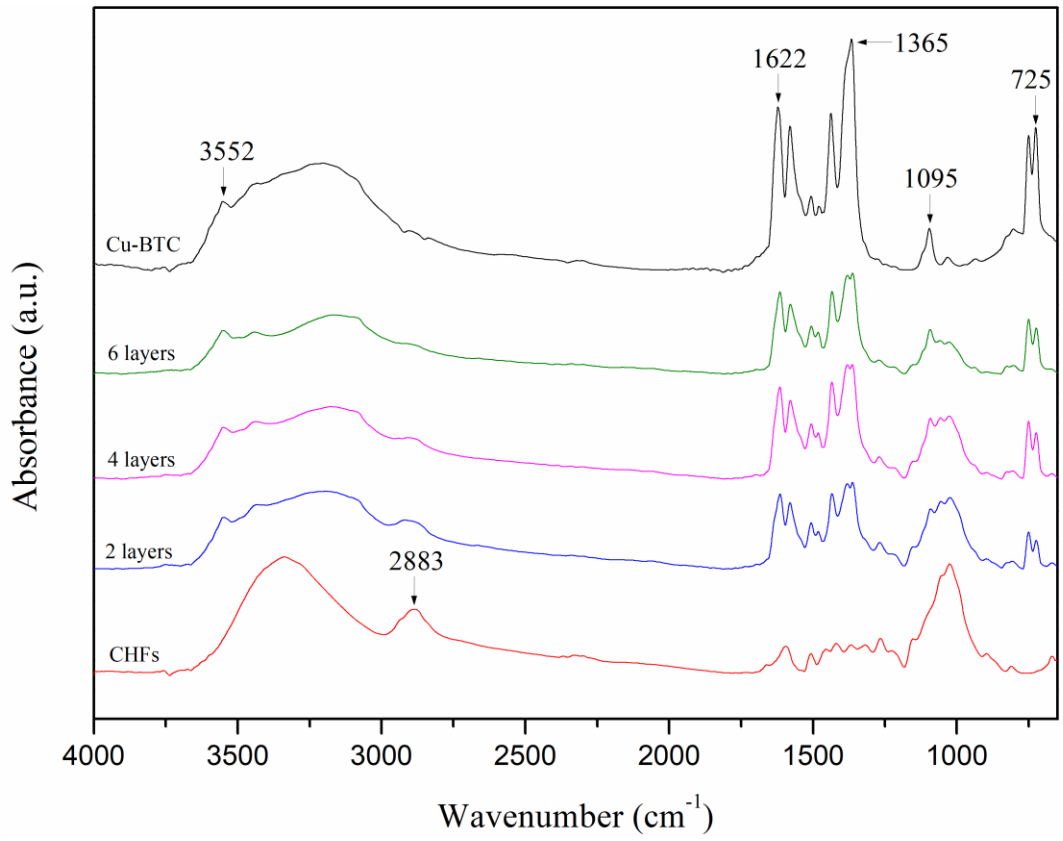

Fig. 2-3 ATR FTIR spectra of Cu-BTC, CHFs, and Cu-BTC@CHFs with different layers

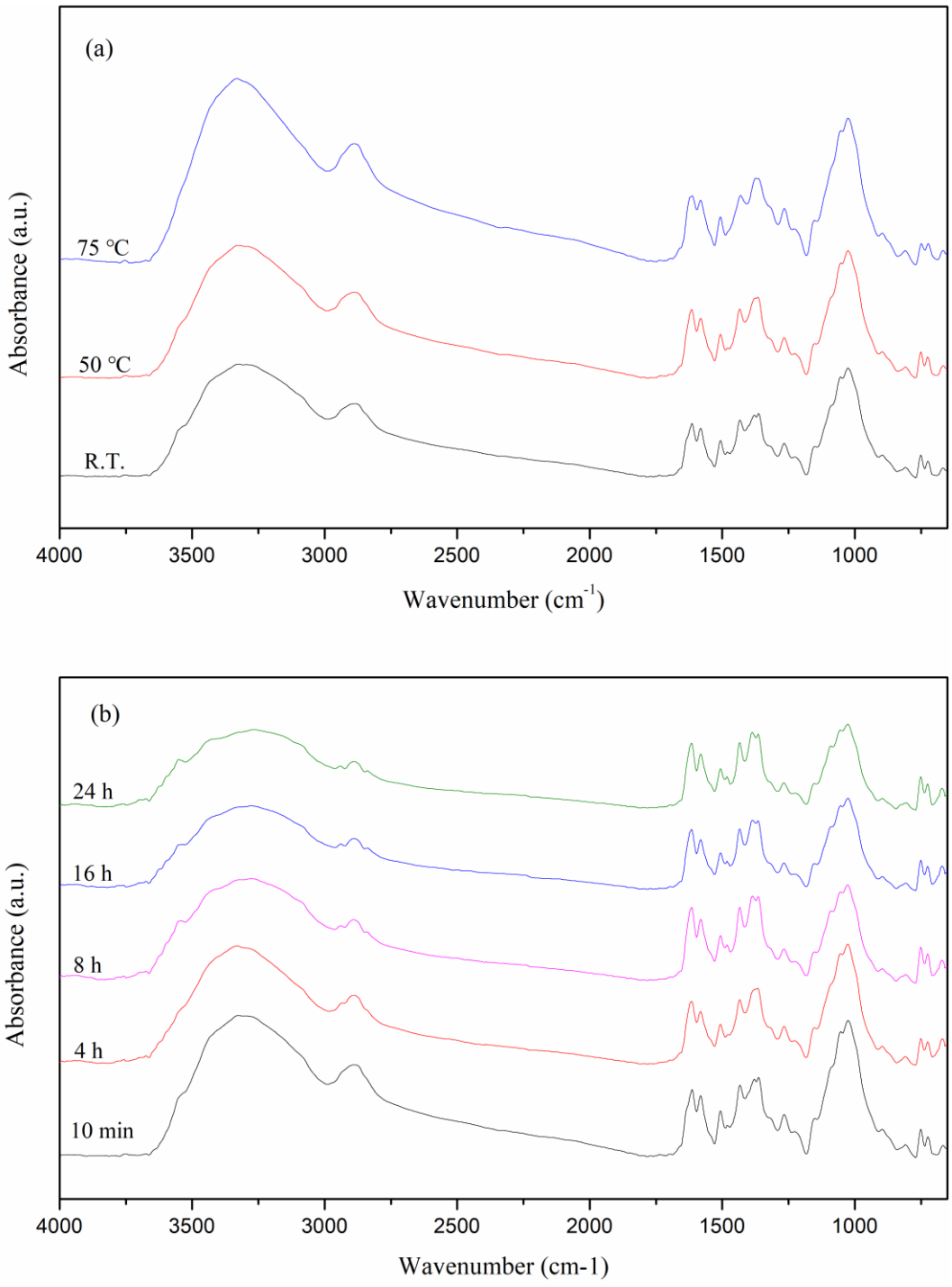

Fig. 2-4 ATR FTIR spectra of Cu-BTC@CHFs prepared at different temperature (a) and different time (b)

In order to confirm the presence of Cu-BTC in the prepared composites, the chemical structure of Cu-BTC@CHFs prepared in different conditions was studied by ATR FT-IR, as shown in Fig. 2-3 and Fig. 2-4. The sharp OH vibration at 3552 cm^{-1} and broad band of absorbed water at 3500 – 3200 cm^{-1} indicate the presence of bound water in Cu-BTC prepared in aqueous solution. The strong absorption bands are observed at 1622 cm^{-1}, 1365 cm^{-1} 1095 cm^{-1}, and 725 cm^{-1}, which represent COO^- asymmetric, COO^- symmetric vibration, C-H in-plane, and C-H out-of-plane bending vibration, respectively, corresponding to BTC coordinated with copper [90, 105, 115]. All these peaks can be found in the spectra of Cu-BTC and Cu-BTC@CHFs prepared in different conditions, which confirm the formation and deposition of Cu-BTC on the carboxymethylated high yield pulp fibers.

As shown in Fig. 2-4(a) and (b), samples of Cu-BTC@CHFs with 1 layer prepared in different temperature and time show similar spectra, but the intensities of CH_2 groups stretching vibration of fibers at 2883 cm^{-1} decreased with extending the preparation time, indicating the preparation time has more effect on Cu-BTC depositing on CHFs than temperature and Cu-BTC@CHFs can be prepared in room temperature. Fig. 2-3 shows the ATR FT-IR spectra of Cu-BTC@CHFs with different layers, the intensities of CH_2 groups of fibers at 2883 cm^{-1} decreased, the intensities of COO^- at 1622 cm^{-1} (asymmetric) and 1365 cm^{-1}(symmetric) and C-H at 1095 cm^{-1} (in-plane) and 725 cm^{-1} (out-of-plane) of Cu-BTC increased with more deposition layers. This suggests that the Cu-BTC film on high yield pulp fibers can be formed and intensified by the layer-by-layer method.

2.3.4 XRD patterns of Cu-BTC@CHFs prepared in different conditions and growth layers

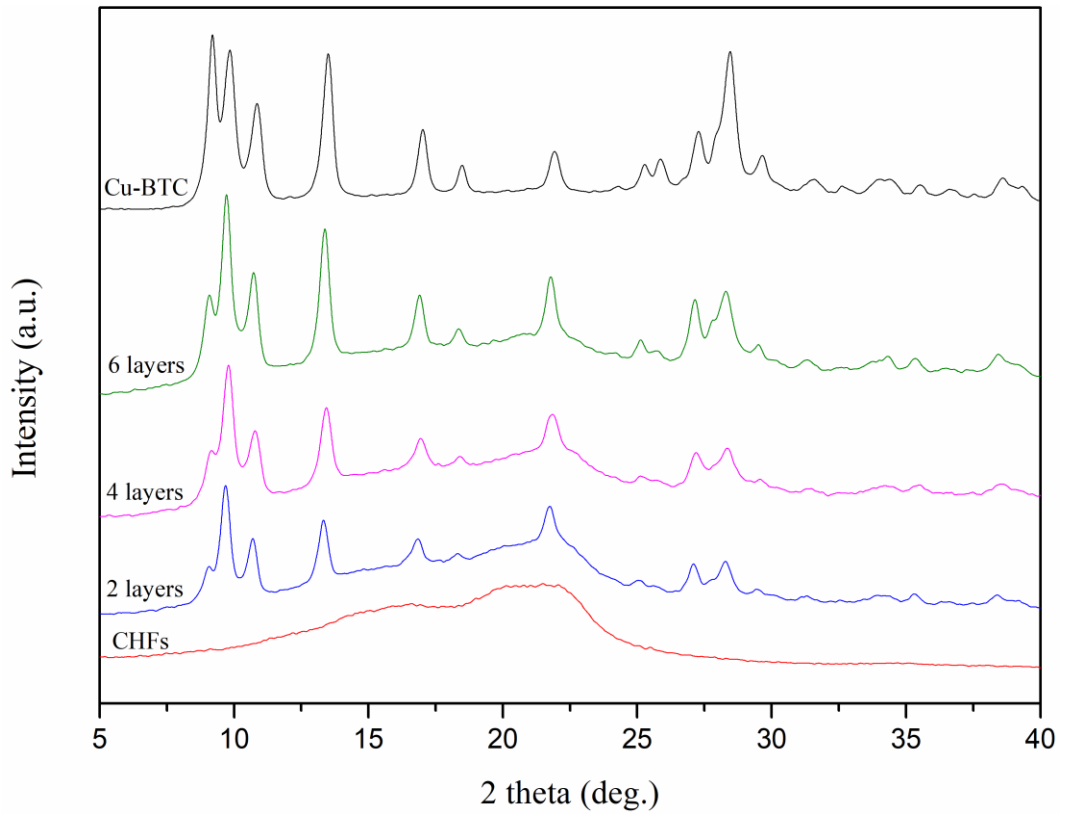

Fig. 2-5 XRD spectra of Cu-BTC, CHFs, and Cu-BTC@CHFs with different layers

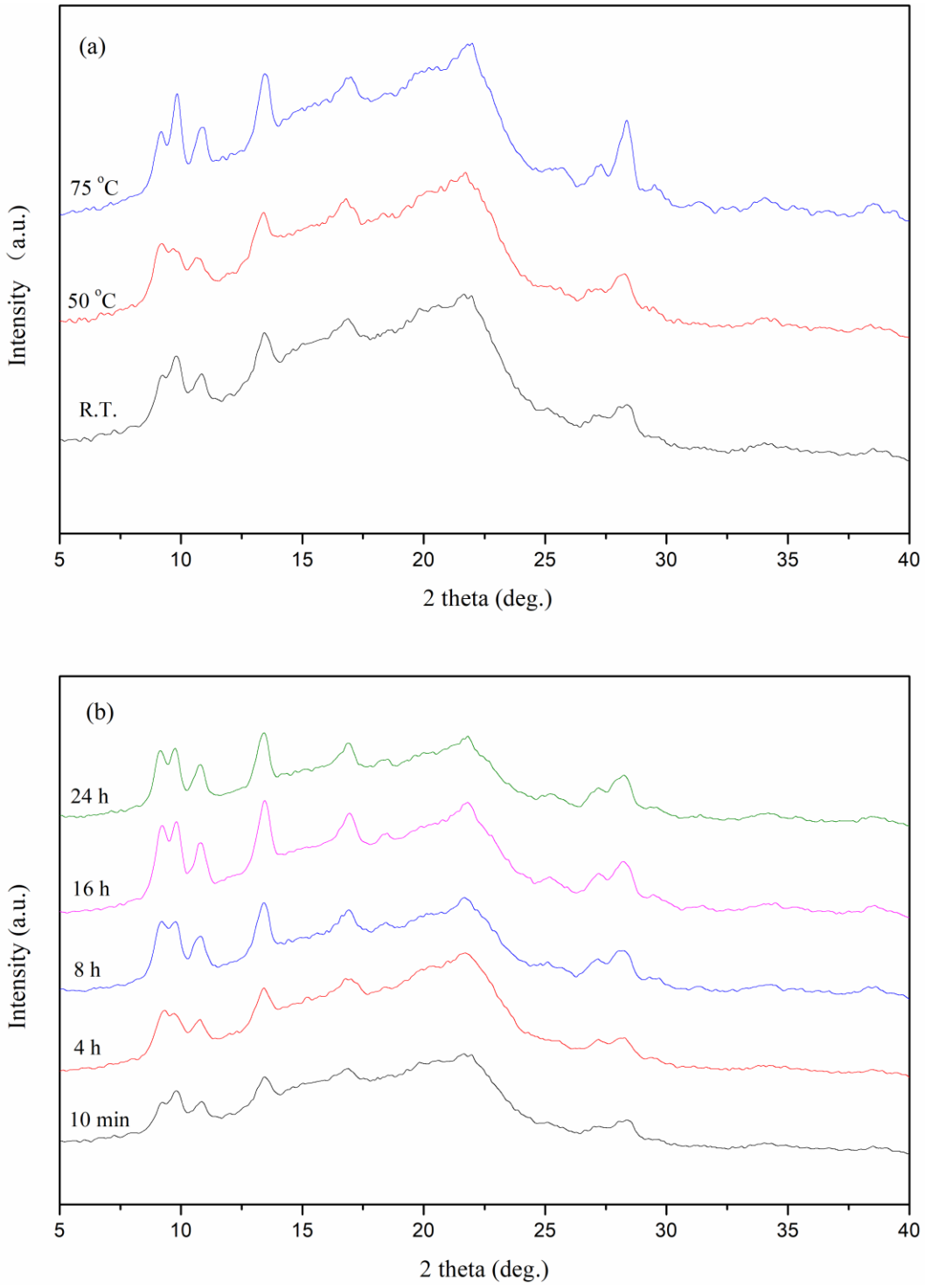

Fig. 2-6 XRD patterns of Cu-BTC@CHFs prepared at different temperature (a) and different time (b)

Cu-BTC metal-organic framework was prepared by using Na_3BTC as linker source and water as the solvent instead of organic solvents such as dimethylformamide and ethanol so that the spent liquor can be easily handling and processing. The synthesized Cu-BTC blue powder was characterized by X-ray diffractometer, as shown in Fig. 2-5 and Fig. 2-6. The major diffraction 2θ peaks observed at 9.7º, 13.4º, 16.9º, 17.4º, 25.1º, 28.3º were associated with Cu-BTC [90, 105, 116]. The presence of peaks at 9.2º and 10.9º and absence of peak at 6.5º indicated that the Cu-BTC prepared in aqueous solution was a partially hydrolyzed phase of Cu-BTC prepared in organic solvents, which is in accordance with the work of Al-Janabi et al. [117] and Álvarez et al. [118] that the structure of crystal prepared in organic solvent will partially degrade when exposed in water. The broad diffraction peaks of CHFs between 15º and 25º are associated with amorphous cellulose, as shown in Fig. 2-5. Both characteristic peaks of Cu-BTC and CHFs can be found in prepared Cu-BTC@CHFs, just with different intensities and the weaker intensity at peak of 9.2º was caused by more time immersion in the water, which further confirmed the growth of Cu-BTC metal-organic framework onto modified HYP fibers.

The effect of preparation temperature and time on the growth of Cu-BTC on fiber surface was also studied by XRD, as shown in Fig. 2-6 (a) and (b). It was noticed that the peak intensities of Cu-BTC@CHFs increased with higher preparation temperature and a longer period of time, but not significantly, which indicated more Cu-BTC deposited onto fiber surface. Although increasing preparation temperature and time can contribute to more Cu-BTC growing onto fibers, it will result in poor efficiency and

more energy consumption. Therefore, the layer-by-layer method was conducted to prepare Cu-BTC@CHFs, the XRD patterns were shown in Fig. 2-5. More characteristic peaks of Cu-BTC were observed when increasing the growth layer, which overlapped with the peaks of CHFs. This can be attributed to more Cu-BTC depositing onto fiber surface and the formation of a thicker Cu-BTC film.

2.3.5 Morphology and deposit ratio analysis

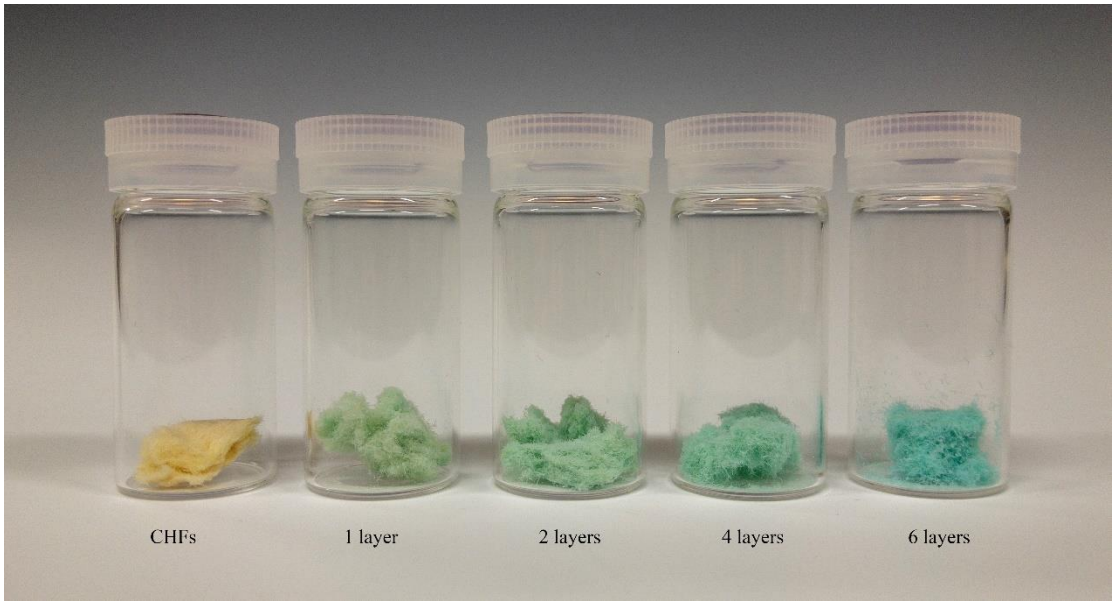

Fig. 2-7 Optical image of CHFs and Cu-BTC@CHFs with different deposit layers (1,2,4,6, from left to right)

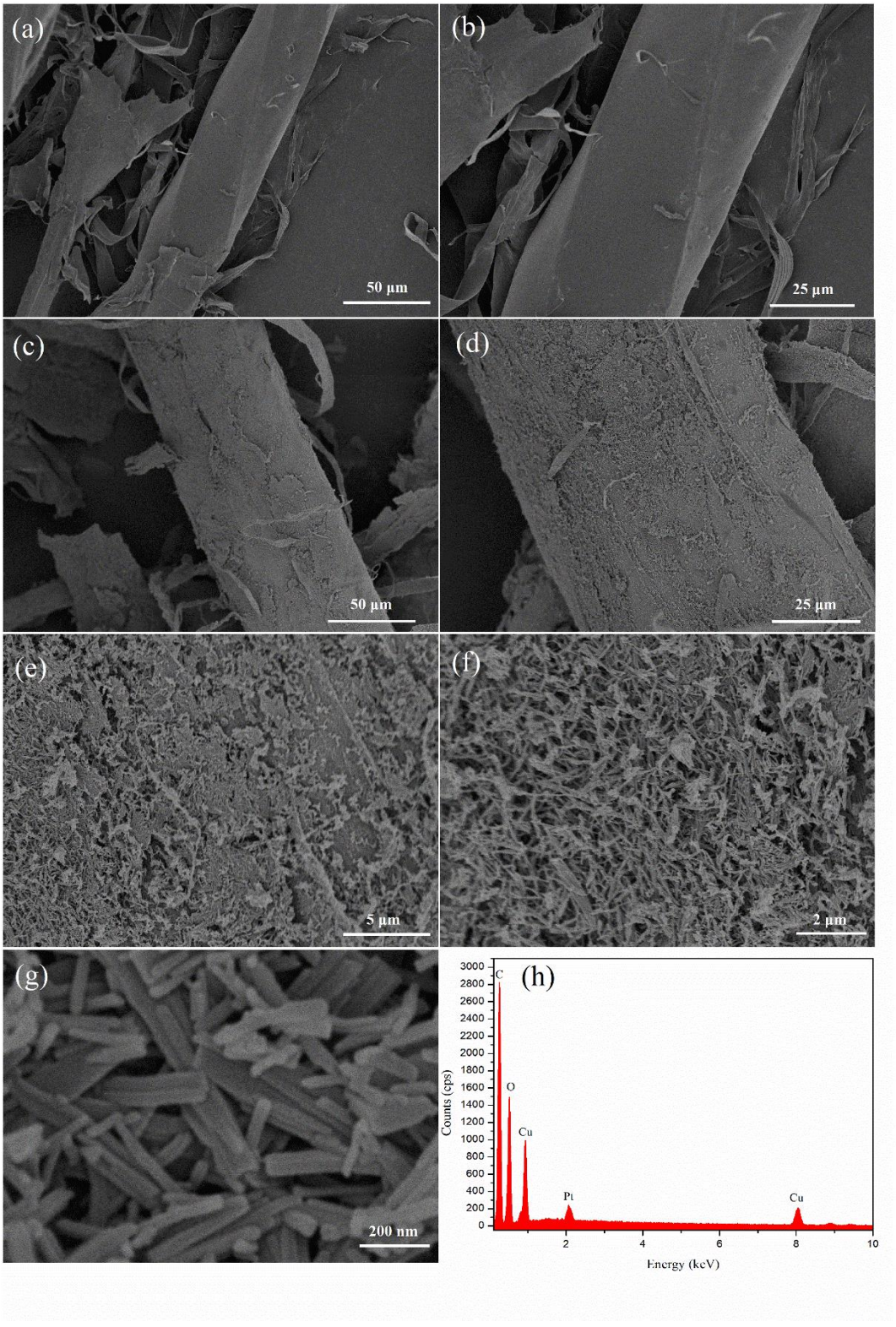

Fig. 2-8 SEM images of CHFs at (a) 500× and (b)1000×, Cu-BTC@CHFs with 6 layers at (c) 500×, (d) 1000×, (e) 5k×, (f) 10k×, and (g) 100k×, and (h) EDS analysis

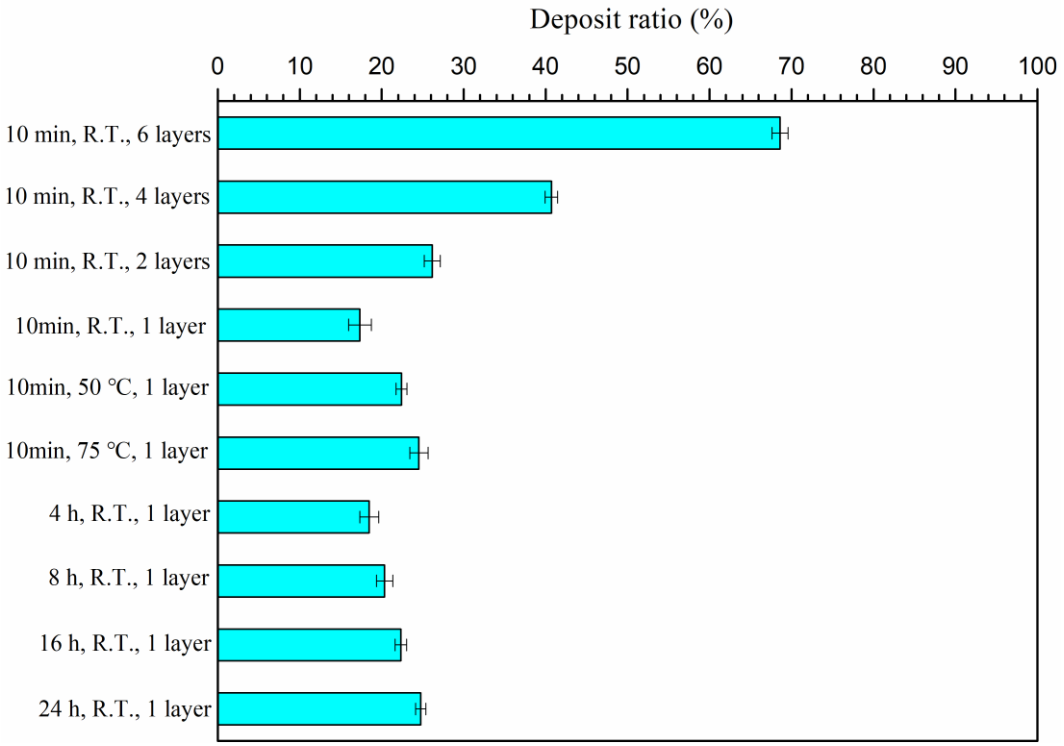

Fig. 2-9 Deposit ratio of Cu-BTC onto CHFs in different preparation condition and growth layers

Fig. 2-7 shows the optical image of CHFs and Cu-BTC@CHFs with different deposit layers, the characteristic blue color of Cu-BTC confirmed its uniform distribution on the fiber surface. The carboxymethylated high yield pulp fibers were changed from yellow to deep blue gradually with increasing the growth layers from one layer to six layers.

To further investigate Cu-BTC depositing on the fiber surface, SEM and EDS analysis was performed on CHFs and Cu-BTC@CHFs with six layers, as shown in Fig. 2-8. The surface of carboxymethylated high yield pulp fibers showed a smooth surface,

shown as Fig. 2-8 (a) and (b). Compared with unmodified CHFs, samples of Cu-BTC@CHFs with 6 layers showed a rough surface, which indicated the Cu-BTC crystals were deposited on fiber surface successfully, as shown in Fig. 2-8 (c) and (d). As for Cu-BTC@CHFs composite at 5 k× and 10 k× in Fig 2-8 (e) and (g), the material surface was covered with particles densely during the growth of Cu-BTC metal-organic framework. These images clearly showed the formation of Cu-BTC crystal particles on the fiber surface with a broad range of sizes. With higher magnification at 100 k in Fig. 2-8 (g), the morphology of prepared Cu-BTC showed a nanorod-like shape, which was different from that made by common synthesis methods in organic solvents with a cubic morphology and the size was also smaller. The Cu-BTC@CHFs composite was also evaluated by SEM-EDS analysis using a copper probe, as shown in Fig 2-8 (h). The EDS result clearly showed a high copper content on the substrate, which further confirmed the growth of Cu-BTC onto the fiber surface.

The deposit ratio of Cu-BTC onto fiber surface prepared in different conditions was also determined, as shown in Fig. 2-9. It revealed that the deposit ratio increased slightly with raising the growth temperature and extending the growth time, but increased dramatically with increasing the growth layers, which is in accordance with the results of ATR FT-IR and XRD. When increasing growth temperature form R.T. to 75 ^{o}C and extending growth time from 10 min to 24 h, the deposit ratios increased from 17.33% to 24.53% and 24.75%, respectively, which was even little lower than the deposit ratio of 2 layers for 26.17%. When continuing to increase the growth layer to six, the deposit ratio was up to 68.59%. These results indicated that increasing growth

time and temperature would enhance the deposit of Cu-BTC on fiber surface at a limited range and increasing the growth layer would be a more effective way.

2.3.6 Stability and gas adsorption capacity analysis

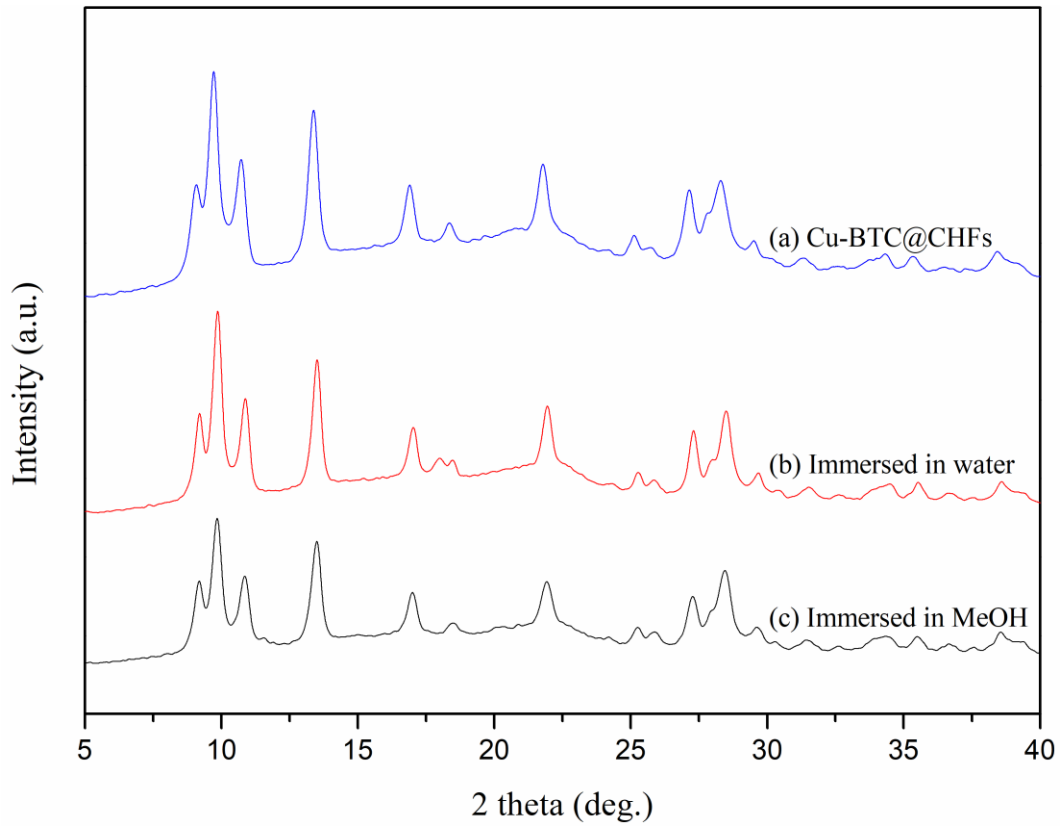

Fig. 2-10 XRD spectra of Cu-BTC@CHFs with 6 layers (a), immersion in water (b), and methanol (c) at R.T. for 24 h

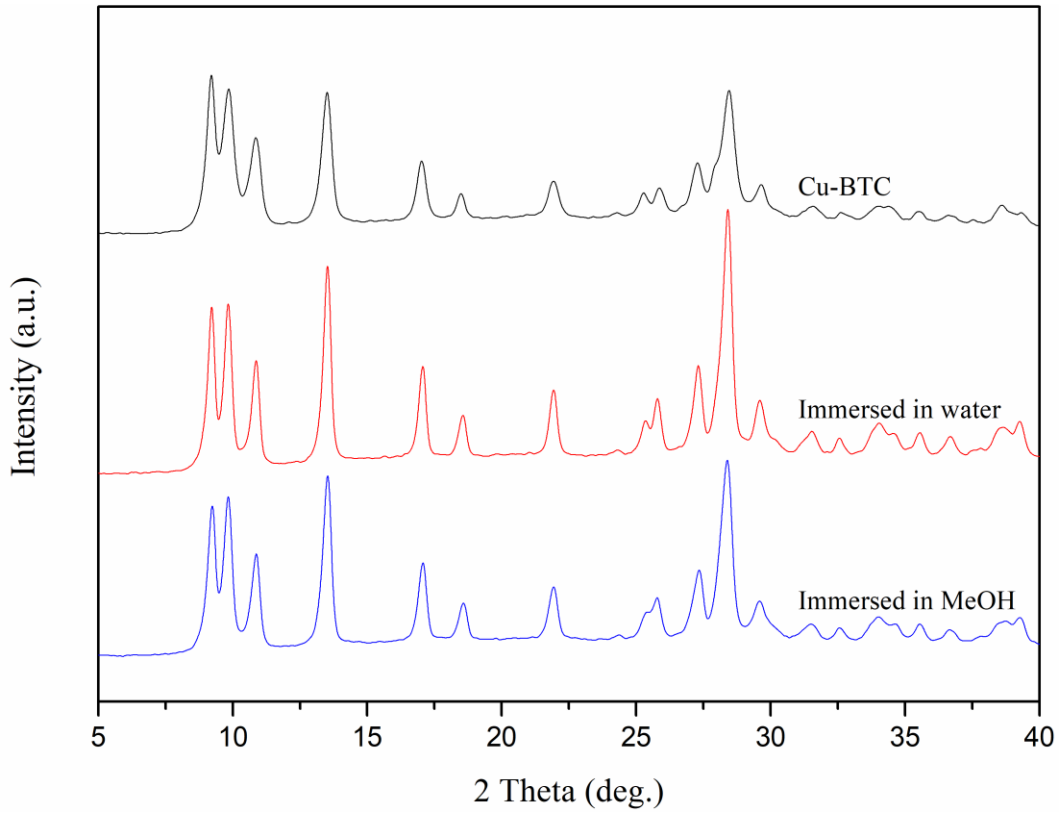

Fig. 2-11 XRD patterns of Cu-BTC prepared in aqueous solution, and immersed in water and methanol for 24 h at R.T., respectively

Table 2-2 Deposit ratio of Cu-BTC@CHFs with 6 layers and immersed in water and methanol for 24 h

Samples	Deposit ratio (%)
Cu-BTC@CHFs	68.59 ± 0.98
Immersed in water	67.00 ± 0.37
Immersed in methanol	65.99 ± 0.45

For industrial practice, simple alcohols are usual solvents, so methanol and water were used in this study to investigate the stability of prepared Cu-BTC@CHFs composite. Samples of Cu-BTC prepared in aqueous solution and Cu-BTC@CHFs with 6 deposit layers of deposited MOFs were immersed in methanol and water for 24 h at R.T. respectively, prior to XRD analysis. The stability of Cu-BTC prepared in water was characterized by XRD, as shown in Fig. 2-11. After 24 h immersed in water and methanol, both the characteristic peaks of Cu-BTC showed a little higher intensity compared with the original as-prepared Cu-BTC, which can be attributed to that after 24 h immersion in water and methanol, some impurities were separated out and the products became purer compared with the original product. Meanwhile, it showed that at the given time (24 h), the product was stable in both water and methanol. And the intensity of product immersed in water was also little higher than that of immersed in methanol, which indicated water was more effective than methanol for purifying Cu-BTC prepared in aqueous solution. Fig. 2-10 and Table 2-2 showed the XRD spectra and deposit ratio of Cu-BTC@CHFs with 6 layers and immersed in water and methanol for 24 h, respectively. As shown in Fig. 2-10, the XRD spectra showed similar peaks, which meant the crystal structures remained the same after immersion in methanol and water. Table 2-2 showed that both the deposit ratio of Cu-BTC immersed in water and methanol for 24 h decreased slightly due to some crystals detaching from the composite in water and methanol, but a little more significant in methanol. In addition, the characteristic peaks of Cu-BTC@CHFs immersed in water showed a little higher intensity than that of immersed in methanol, which further indicated the currently

prepared Cu-BTC@CHFs composites were likely to be more stable in pure water than methanol. This can be attributed to that the products were already immersed in water for a long-time during synthesis and washing process and became stable in pure water.

Table 2-3 Specific surface area and pore volume of Cu-BTC, Cu-BTC@CHFs with 6 layers and CHFs

Samples	BET Specific surface area (m^2/g)	Pore volume (cm^3/g)
Cu-BTC	43.782	0.253
Cu-BTC@CHFs	28.422	0.132
CHFs	1.997	0.028

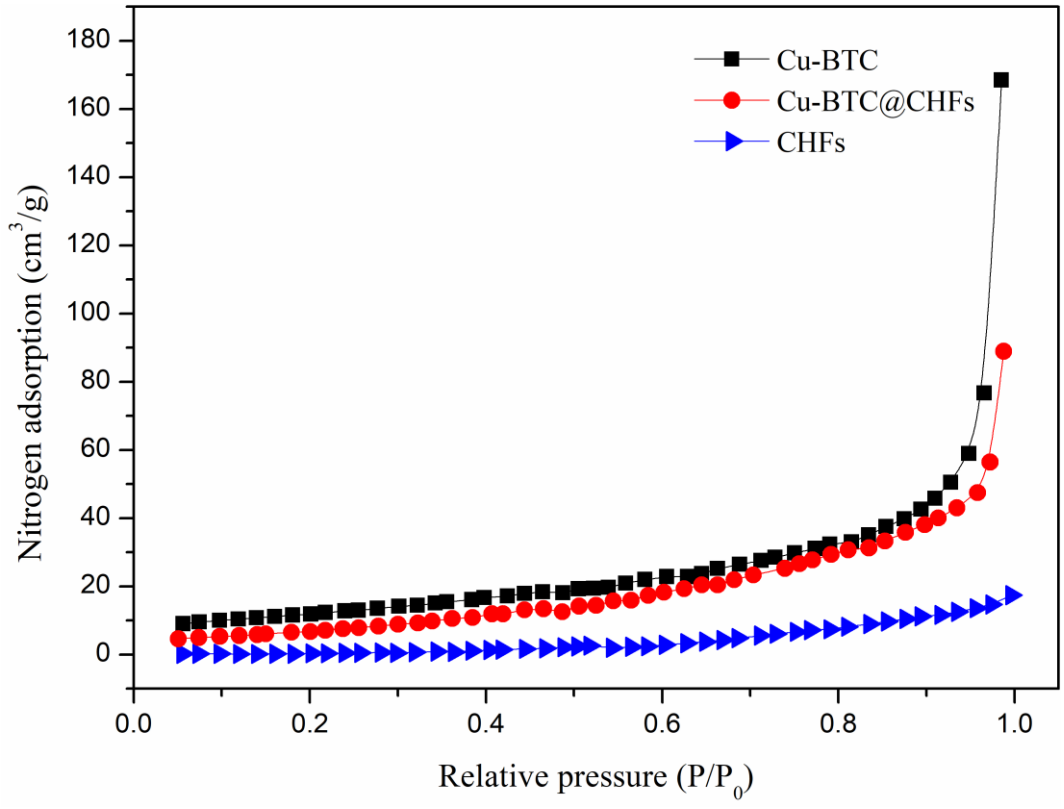

Fig. 2-12 Nitrogen adsorption isotherms of Cu-BTC, Cu-BTC@CHFs with 6 layers, and CHFs

Larger specific surface area is one of the most important properties of metal-organic framework porous material, so the gas adsorption capacity of prepared Cu-BTC@CHFs with 6 layers was analyzed by nitrogen adsorption at 77 K, as shown in Tab. 2-3 and Fig. 2-12. The synthesized Cu-BTC at aqueous solution had as a small BET specific surface (43.782 m^2/g, Tab. 2-3), this could be explained by the fact that Cu-BTC synthesized in water is a partially hydrolyzed phase of common Cu-BTC synthesized in organic solvents, but the value is greatly higher than Zn-BDC metal-organic framework synthesized in water with a specific surface area value of 11.98 m^2/g

[108]. As shown in Tab. 2-3, both BET specific surface area and pore volume of Cu-BTC@CHFs increased significantly compared with unmodified CHFs contributed by the growth of Cu-BTC crystal. As for the N_2 adsorption isotherms shown in Fig. 2-12, the adsorption curves of Cu-BTC and Cu-BTC@CHFs increased rapidly beyond 0.9 p/p_0, indicating a remarkable capillary condensation effect on samples [119]. The adsorption capacity tendency of Cu-BTC crystals was higher than Cu-BTC@CHFs, followed by unmodified CHFs, which was consistent with the tendency of specific surface area and pore volume in Tab. 2-3. Thus, the gas adsorption capacity of Cu-BTC@CHFs was promoted by growth of Cu-BTC onto fiber surface.

The synthesized Cu-BTC@CHFs composites in aqueous solution, making full use of lignocellulosic fibers and easy for liquid waste treatment, equipped with a copper element and certain specific surface area will have potential application with the advantage of being more economical and environmental-friendly in antimicrobial and adsorption, which should be further studied.

2.4 Conclusion

This work demonstrates a strategy of preparing Cu-BTC metal-organic framework onto lignocellulosic fibers in aqueous solution by a layer-by-layer method. The lignocellulosic fibers were first carboxymethylated to improve the number of nucleation sites of Cu-BTC crystal growth, then using sodium trimesic as the linker sources to synthesize Cu-BTC onto fiber surface in water by layer-by-layer method, resulting in a uniform distribution of MOF on the fiber surface. The synthesized Cu-

BTC in water was partially hydrolyzed phase of that prepared in organic solvents. The deposit ratio increased slightly with raising growth temperature and extending growth time but increasing remarkably with more growth layers. The prepared Cu-BTC@CHFs composites were more stable in pure water than methanol due to the longtime immersion of water-based synthesis and washing process. The specific surface area of synthesized Cu-BTC@CHFs had a significant promotion compared with unmodified fibers, showing a certain gas adsorption capacity, which can be further used as a porous material.

Chapter 3

A comparative study of depositing Cu-BTC metal-organic framework onto cellulosic filter paper via different procedures

3.1 Introduction

Cellulosic fiber, derived from abundant plant resources, has received large attention in various fields due to its versatility, low cost, low specific gravity, sustainability, biodegradability, etc. [64, 120] Among all kinds of cellulose-based materials, cellulosic fiber is a potential high-value substrate, widely applied in many fields, such as super-capacitors [121, 122], metal nanoparticles [123, 124], and cationic polyelectrolytes [125].

In recent years, several studies have been performed on depositing metal-organic frameworks onto cellulosic fibers to mold MOF crystalline powder for specific applications [66]. MOFs are a new sort of porous coordinate polymer with exceptionally high surface area and tunable pore size [7, 13]. To deposit MOFs on the cellulose fibers, the hydroxyl groups of cellulose can be subjected to chemical modifications such as carboxymethylation, TEMPO or hydrogen peroxide oxidation, resulting in negative sites for anchoring metal ions and then the subsequent growth of MOFs.

However, the procedures for depositing metal-organic frameworks onto cellulose-based materials varied a lot in different studies, which led to different end properties of the resultant products. In the initial researches, a one-pot procedure was employed to

immobilize metal-organic frameworks onto cellulose fibers. In these studies, either the cellulose fibers were immersed in metal ions precursor for certain time then organic linkers were added or the fibers were immersed in the solutions containing all required chemicals [72, 88, 92, 105]. However, this procedure was time-consuming (up to 24h), and had a lower MOFs deposition ratio. Moreover, the final products were not subjected to any treatment to remove the unreacted chemicals.

Richardson et al. [126] prepared MOFs layers around cellulose nanocrystal filaments using an altered one-port procedure. The authors varied the ratio of precursors using different raw materials and chemical dosages. To increase the deposit ratio of MOFs crystals onto selected substrates and reduce the preparation time, some improved procedures were performed, for instance, layer-by-layer procedure [102, 127], two-step procedure (taking out the substrate from metal ions precursor before immersing in organic linkers solution) [69], and integrated procedure [90]. The particle size and gas adsorption capacity varied among these diverse preparation procedures, so a comparative study concerning the preparation procedures of depositing MOFs onto cellulose-based material substrate is necessary.

In this work, the key characteristics and properties of Cu-BTC metal-organic frameworks deposited onto commercial filter paper prepared via four different procedures (one-pot, two-step, LbL-org, LbL-wtr-org) were comparatively studied. The prepared products were characterized by SEM, EDS, ATR FT-IR, and XRD. The deposit ratio and gas adsorption capacity were also evaluated.

3.2 Experimental Section

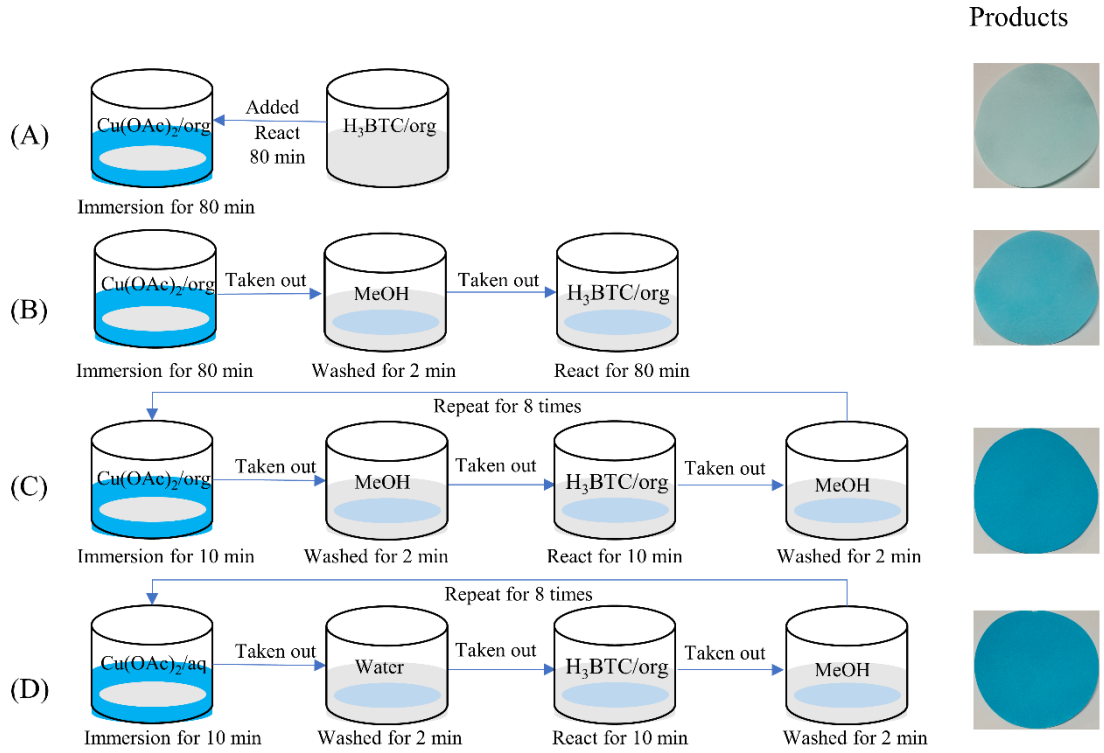

Fig. 3-1 Schematic of depositing Cu-BTC onto carboxymethylated filter paper in different procedures

3.2.1 Materials

Commercial qualitative filter papers (No. 2, 55 mm diameter, 132 g/m^2) purchased from Advantec, were used as received. Copper (II) acetate monohydrate ($Cu(OAc)_2 \cdot H_2O$), 1,3,5-benzene-tricarboxylic acid (H_3BTC), sodium chloroacetate ($ClCH_2COONa$), dimethylformamide (DMF), ethanol (EtOH), methanol (MeOH), sodium hydroxide (NaOH), and methylene blue were purchased from FUJIFILM Wako Pure Chemical Corporation, Japan. All chemicals were used as received without any

further purification. Lab-made deionized water was used throughout all the experiments.

3.2.2 Carboxymethylation of filter paper

One piece of cellulosic filter paper was immersed in 30 mL 1 M sodium chloroacetate solution prepared by 15% (w/v) sodium hydroxide solution for 2 h at 50 ^{o}C. The beaker was shaking and filter paper was turned over every 30 min to ensure uniform carboxymethylation treatment. The carboxymethylated filter paper (CMP) was then washed thoroughly with deionized water until the rinsed water reached a neutral pH. Finally, the carboxymethylated cellulosic filter paper was air-dried at room temperature. The carboxyl content determination of original and carboxymethylated filter paper was performed by the methylene blue method, as described in part 2.2.

3.2.3 Preparation of Cu-BTC and Cu-BTC@CMP with different procedures

Cu-BTC metal-organic framework was prepared following a modified procedure reported elsewhere [10]. Briefly, Copper (II) acetate monohydrate ($Cu(OAc)_2 \cdot H_2O$, 860 mg, 4.31 mmol) was mixed in 30 mL of DMF/EtOH/H_2O (1:1:1), then 1,3,5-benzene-tricarboxylic acid (H_3BTC, 500 mg, 2.38 mmol) dissolved in 30 mL of the same solvent was added and stirred at room temperature for 1 h. The final product was subjected to a centrifugation-redispersion process using the same solvent as above for three times, and vacuum dried at 50 ^{o}C for overnight.

Cu-BTC deposited onto carboxymethylated filter paper (Cu-BTC@CMP) was prepared by different procedures, as shown in Fig. 3-1, described as follows,

(A): one piece of CMP was immersed in $Cu(OAc)_2 \cdot H_2O$ (860 mg) mixed in 30 mL

organic solution (DMF/EtOH/H_2O, 1:1:1) for 80 min. Thereafter, H_3BTC (500 mg) dissolved in 30 mL of the same organic solution was added, reacting at R.T. for 80 min, referred as one-pot procedure.

(B): one piece of CMP was immersed in $Cu(OAc)_2 \cdot H_2O$ (860 mg) mixed in 30 mL organic solution (DMF/EtOH/H_2O, 1:1:1) for 80 min, taken out and immersed in 30 mL MeOH for a 2 min wash, and then transferred to H_3BTC (500 mg) dissolved in 30 mL of the same organic solution at room temperature (R.T.) for 80 min, referred as two-step procedure.

(C): one piece of CMP was immersed in $Cu(OAc)_2 \cdot H_2O$ (860 mg) mixed in 30 mL organic solution (DMF/EtOH/H_2O, 1:1:1) for 10 min, taken out and immersed in 30 mL MeOH for 2 min wash, then transferred to H_3BTC (500 mg) dissolved in 30 mL of the same organic solution, at R.T. for 10 min and taken out, subjected to another 2 min MeOH wash. The resultant product was subjected to this process 8 times, referred as Layer-by-Layer-organic (LbL-org) procedure.

(D): one piece of CMP was immersed in 30 mL aqueous solution of $Cu(OAc)_2 \cdot H_2O$ (860 mg) for 10 min, taken out and immersed in 30 mL H_2O for 2 min, then transferred to H_3BTC (500 mg) dissolved in 30 mL of organic solution (DMF/EtOH/H_2O, 1:1:1), reacted at R.T. for 10 min and taken out, immersed in 30 mL MeOH for a 2 min wash. The resultant product was subjected to this process 8 times, referred as Layer-by-Layer-water-organic (LbL-wtr-org) procedure.

All the products after preparation through different procedures were ultrasonically treated for 2 min to remove unreacted chemicals and Cu-BTC not deposited on the

fibers, and then immersed in water, DMF, EtOH for 30 min, respectively, vacuum dried at 50 ^{o}C overnight.

The deposit ratio of Cu-BTC crystal grown onto carboxymethylated filter paper was calculated by the weight difference between CMP and Cu-BTC@CMP.

3.2.4 Characterization

A Fourier transform infrared spectrometer with attenuated total reflectance (ATR) mode (Nicolet 6700, Thermo Fisher Scientific Corp, Japan) under the scanning condition of 128 scans at a resolution of 4 cm^{-1} was used for each sample to obtain the IR spectra. Crystalline phase analysis was performed in an X-ray diffractometer (XRD, Rigaku Corp) using a Cu (λ=0.15418) standard target, from 5^{o} to 40^{o} at a scanning spend of 2.5^{o}/min. The operational current and voltage were 40 mA and 40 kV respectively. The surface morphologies of samples coated with platinum for 30 s were observed by a Field emission scanning electron microscopy (FESEM, S4800, Hitachi, Japan) with an energy-dispersive X-ray spectroscopy (EDS) accessary. The average particle size was calculated manually by marking the crystal diameter length in ImageJ software. Over 150 Cu-BTC crystals in one SEM image were used to calculate the average particle size and particle size distribution. The gas adsorption capacity was investigated by a surface area analyzer (NOVA 4200e, Quantachrome Instrument Corp). The samples were degassed at 80 ^{o}C for 4 h and then the gas adsorption measurements were performed using N_2 gas as the adsorption source at 77 K.

3.3 Results and discussion

3.3.1 Carboxymethylation of cellulosic filter paper

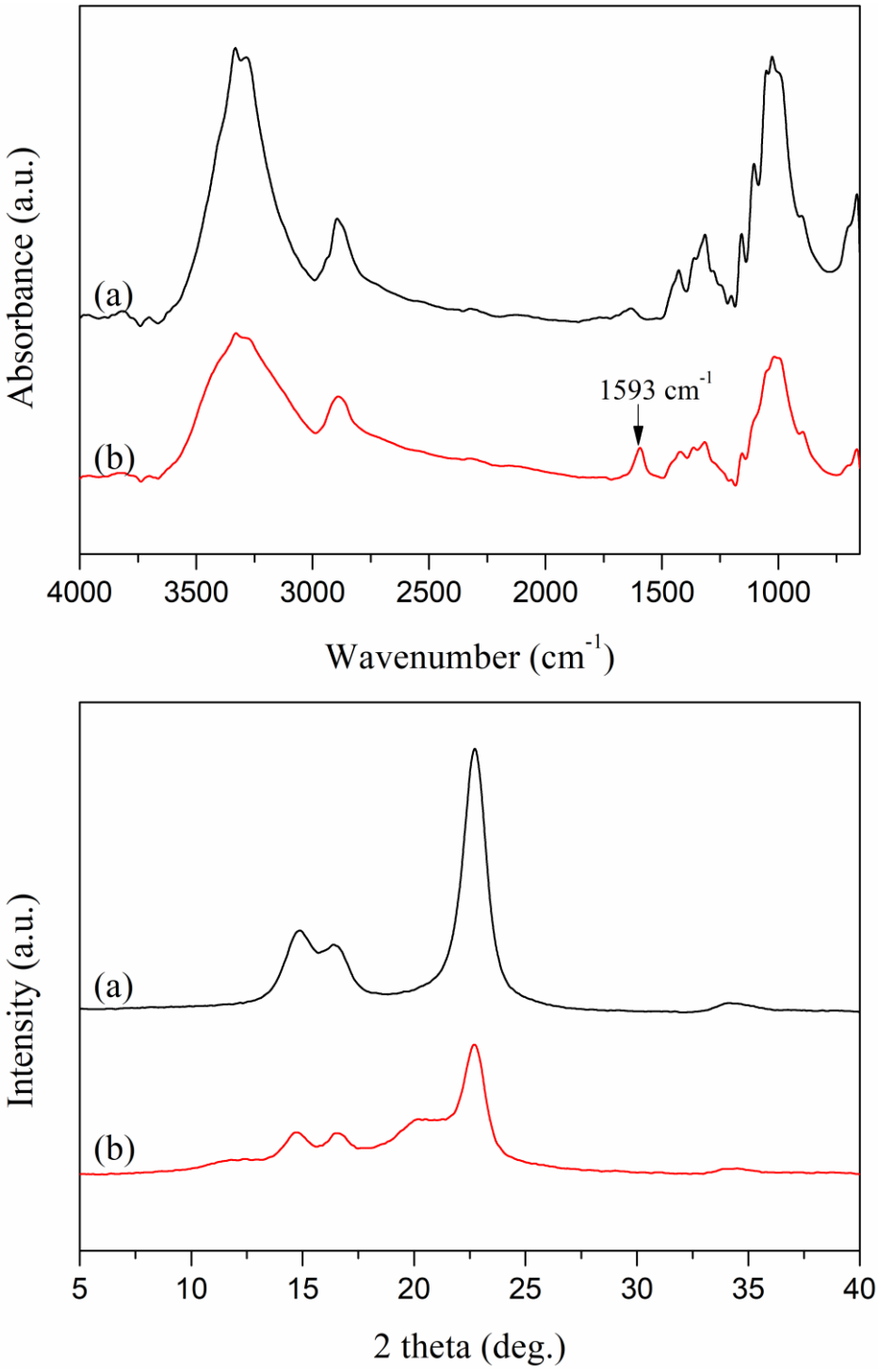

Fig. 3-2 ATR FT-IR spectra (top) and XRD patterns (bottom) of original (a) and carboxymethylated (b) filter paper

Table 3-1 Carboxyl content of original and carboxymethylated filter paper (CMP)

Samples	Carboxyl content (mmol/kg)
Original filter paper	5 ± 0
CMP	150 ± 2

Cellulosic filter paper is a representative cellulose-based material that contains abundant hydroxyl groups, which can be carboxymethylated as a substrate for Cu-BTC metal-organic framework growth. This was conducted by a classic carboxymethylation of filter paper with sodium chloroacetate using sodium hydroxide as the catalyst. The resultant carboxymethylated filter paper cellulose surface was functionalized with carboxyl groups, which was confirmed by IR spectra and XRD patterns compared to unmodified filter paper, as shown in Fig. 3-2. An absorbance peak at 1593 cm^{-1} was found in the ATR FR-IR spectrum of carboxymethylated filter paper, indicating the presence of C=O stretching band. The result was in accordance with the carboxyl content of original and carboxymethylated filter paper, which increased from 5.16 ± 0.15 to 148.98 ± 1.75 mmol/kg, as shown in Table 3-1. Besides, in XRD patterns, the characteristic broad peaks at 2 theta around 15° and 22° of cellulose I were detected, which illustrates that the main component of filter paper cellulose remained intact [128].

Therefore, a suitable material modified with negative carboxylate sites as the substrate for binding Cu^{2+} and then an accelerated growth of Cu-BTC was obtained.

3.3.2 Morphology analysis and deposit ratio

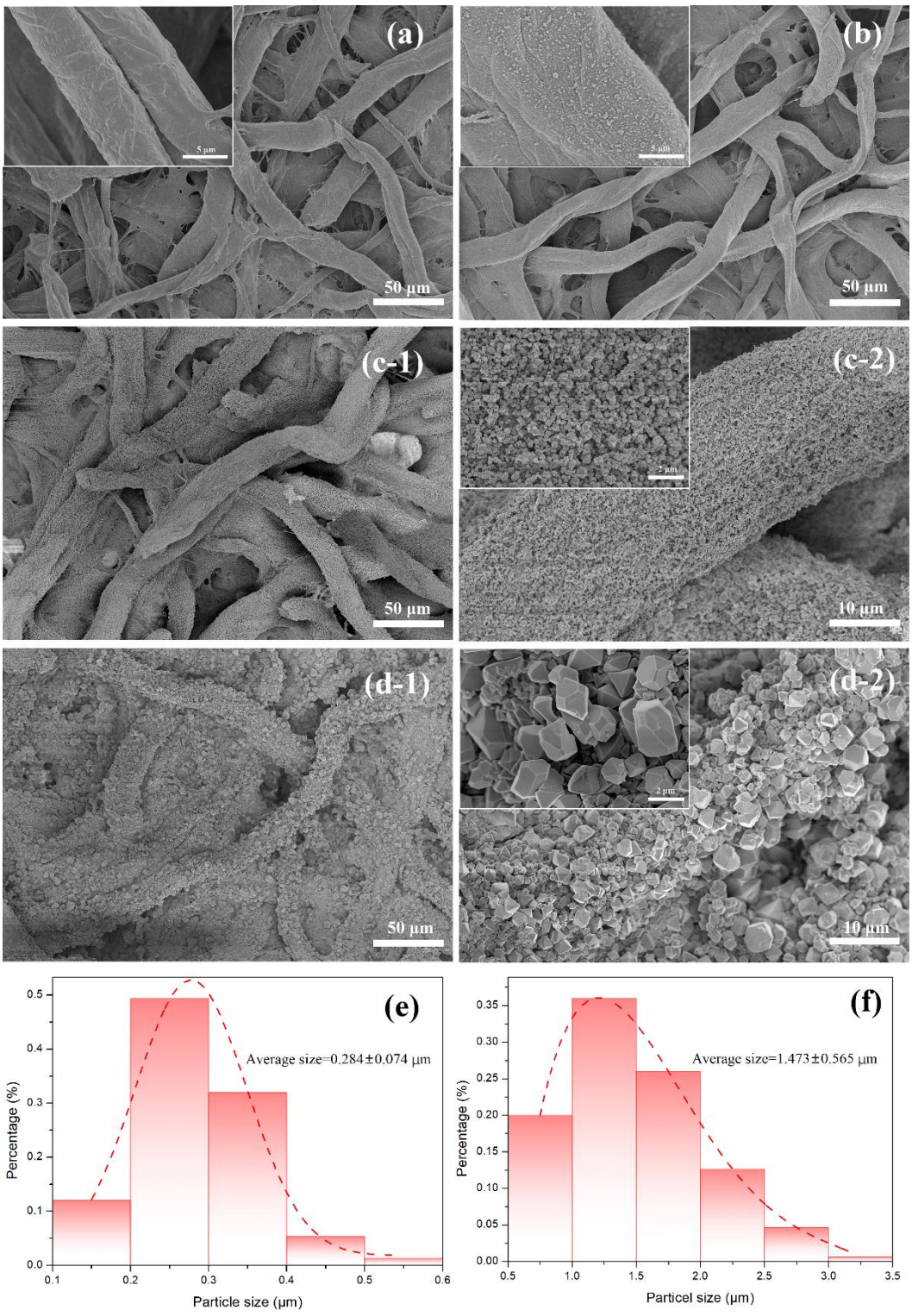

Fig. 3-3 SEM images of (a) one-pot synthesis at 400× with inset at 5k×, (b) two-step procedure at 400× with inset at 5k×, (c-1) LbL-org at 400×, (c-2) LbL-org at 2k× with inset at 10k×, (d-1) LbL-wtr-org at 400×, and (d-2) LbL-water-org at 2k× with inset at 10k×; (e) and (f) particle size distribution of LbL-org and LbL-wtr-org

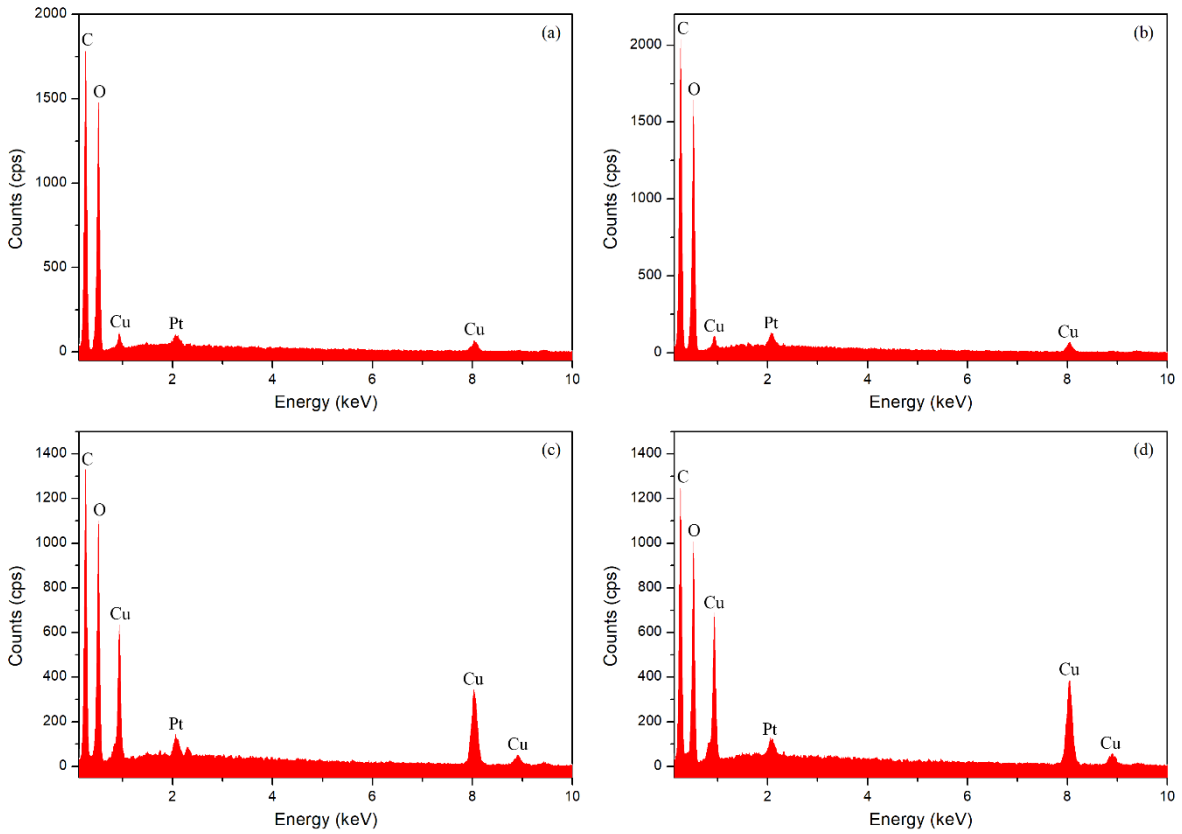

Fig. 3-4 EDS analysis of Cu-BTC@CMP prepared by different procedures: (a) one-pot, (b) two-step, (c) LbL-org, and (d) LbL-wtr-org

Table 3-2 Deposit ratio of Cu-BTC onto carboxymethylated filter paper prepared by different procedures

Procedures	Deposit ratio (%)
One-pot	1.31 ± 0.06
Two-step	4.23 ± 0.63
LbL-org	31.49 ± 3.46
LbL-wtr-org	39.38 ± 1.11

The characteristic blue color of Cu-BTC metal-organic frameworks was distributed uniformly on the filter paper surface, but different color intensities were obtained through different preparation procedures, (as shown in Fig. 3-1 products column). With one-pot procedure, the color of carboxymethylated filter paper changed from white to mild light blue, which is in accordance with a previous research on depositing Cu-BTC onto carboxymethylated cotton surface [105]. With the two-step procedure, the color turned light blue, however, with LbL-org and LbL-wtr-org preparation procedures, Cu-BTC@CMP showed a dark blue color.

The Cu-BTC@CMP samples prepared via different procedures were further characterized by SEM and EDS, as shown in Fig. 3-3 and Fig. 3-4, respectively. The surface of sample prepared by one-pot procedure showed almost no Cu-BTC crystals, while the sample prepared by two-step procedure with the same chemical utilization showed obvious Cu-BTC crystals on the filter paper surface, as shown in Fig. 3-3(a)

and Fig. 3-3(b). Therefore, it can be assumed that the Cu-BTC crystals have a tendency to grow in the main solution rather than on the paper substrate surface with the precondition of the same chemical dosage, although the negatively charged filter paper substrates can immobilize the positively charged Cu^{2+} precursors. This result was consistent with the growth Cu-BTC on porous α-Alumina substrate [110]. To further apply this supposition and achieve a higher amount of Cu-BTC crystals deposition, a layer-by-layer procedure was used (LbL-org). Compared with one-pot and two-step procedures, the layer-by-layer preparation procedure of Cu-BTC@CMP products showed a remarkable mass of Cu-BTC crystals on the filter paper fiber surface, which were distributed densely and uniformly, as shown in Fig. 3-3(c-1) and Fig. 3-3(c-2) with different magnifications. Both the Cu^{2+} and BTC^{3-} solutions were mainly organic solvents (DMF and EtOH), but the actual reaction was performed in BTC^{3-} solution and the $Cu(OAc)_2 \cdot H_2O$ was more easily dissolved in water. So, in order to reduce the dosage of organic solvents, we dissolved Cu^{2+} in deionized water and BTC^{3-} in organic solvents and prepared the products using layer-by-layer procedure (LbL-wtr-org), as described in the experimental part. The SEM images of LbL-wtr-org sample with various magnifications are shown in Fig. 3-3(d-1) and Fig. 3-3(d-2). As with the samples prepared by LbL-org procedure, the carboxymethylated filter paper surface was densely covered with a large mass of Cu-BTC crystals, but the surface was rougher. The particle size of products prepared by LbL-org procedure (0.284μm) was smaller than that by LbL-wtr-org procedure (1.473 μm), as shown in Fig. 3-3(d) and Fig. 3-3(f). It indicates that the particle size distribution of LbL-org was more concentrated, with uniformly

distributed Cu-BTC crystals on the substrate surface compared to the LbL-wtr-org procedure.

The larger size of Cu-BTC crystals deposited on the substrate prepared by LbL-wtr-org procedure can be explained by a relatively higher water content on the Cu-BTC crystals forming sites. In the Lbl-wtr-org procedure, the filter paper is immersed in Cu^{2+} aqueous solution for 10 min and washed in water for 2 min in each growth circle. Due to this treatment, even after taking the paper out of water, a small amount of water may still remain attached on the paper surface. When reacting with BTC^{3-} in the organic solution, a higher water content will result in larger size of Cu-BTC crystals [129].

The products prepared by different procedures were also characterized by SEM-EDS analysis using a copper element probe, as shown in Fig. 3-4, as well as the deposit ratio of Cu-BTC onto the paper surface, as shown in Table 3-2. The EDS result clearly showed a much higher copper content in the LbL-org and LbL-wtr-org products, compared to one-pot and two-step products, which further confirmed a larger amount of Cu-BTC deposited on the paper substrate prepared by layer-by-layer method. The difference of deposited amount between one-pot and two-step procedures, as well as between LbL-org and LbL-wtr-org procedures was too small, so it's difficult to indicate the difference in EDS analysis, as shown in Fig. 3-4(a) and (b), as well as Fig. 3-4(c) and (d). The deposit ratio results in Table 3-2 showed that when using two-step procedure, the deposit ratio increased from 1.31% in the one-pot procedure to 4.23%, but a remarkable yield increase was achieved in layer-by-layer procedures, reaching up to 31.49% in LbL-org and 39.38% in LbL-wtr-org, respectively. The deposit ratio result

of each preparation procedure was corresponding to other studies, for instance, 0.88% of copper element weight using one-pot procedure [105], 80 mg/g (8%) of Cu-BTC weight using two-step procedure [69], 31.64% of Cu-BTC weight using layer-by-layer procedure [102]. Although the studies employed different cellulose-based substrates, pretreatment of the materials, preparation time, and rinse procedures, the values of deposit ratio agreed with our results. Cu^{2+} ion is more easily to be anchored on carboxymethylated filter paper surface in aqueous solution, which explains the higher deposit ratio of products prepared by LbL-wtr-org procedure than that of LbL-org procedure.

3.3.3 IR analysis

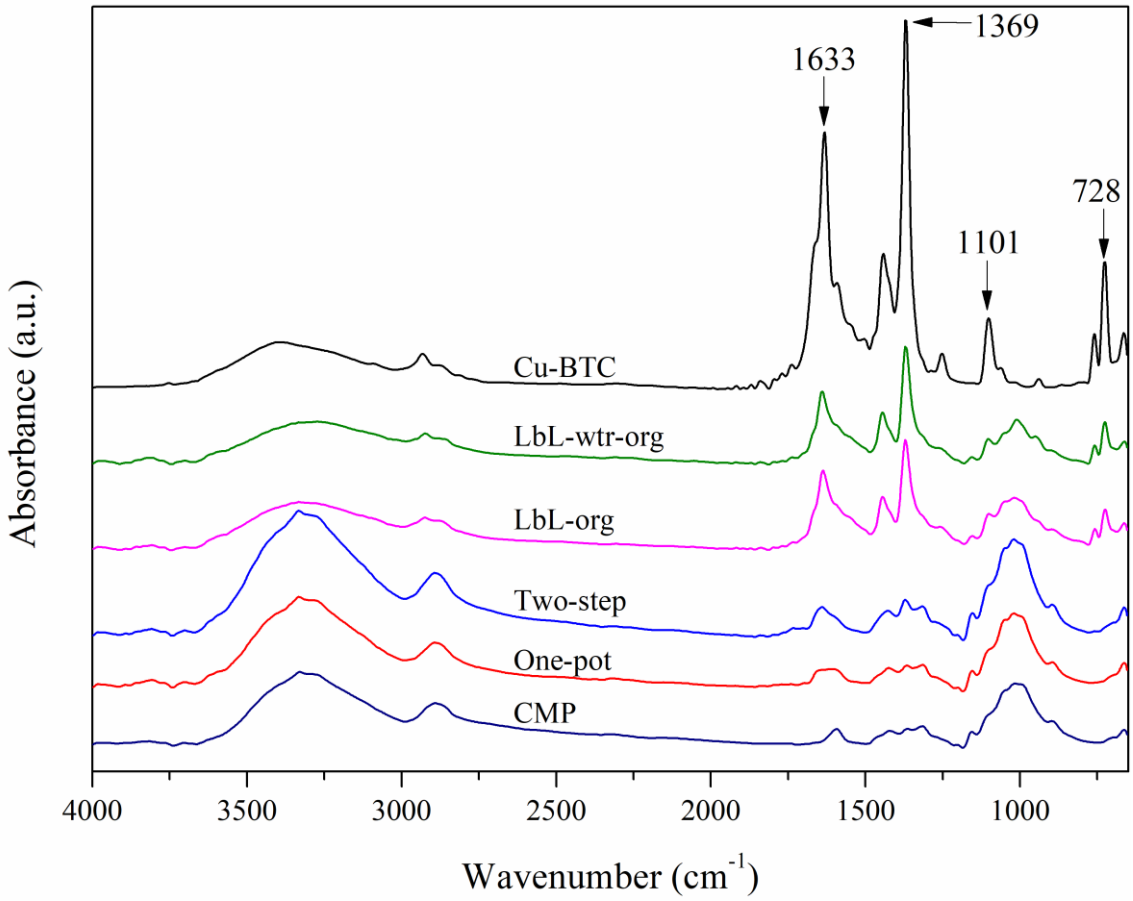

Fig. 3-5 ATR FT-IR spectra of CMP, Cu-BTC and Cu-BTC@CMP prepared by different procedures

In order to further prove the presence of Cu-BTC crystals deposited on carboxymethylated filter paper and compare the difference of products prepared by different procedures, the chemical structure analysis was conducted by ATR FT-IR, as shown in Fig. 3-5. The IR spectrum of Cu-BTC displayed the characteristic bands at 1633 cm^{-1}, 1369 cm^{-1}, 1101 cm^{-1}, and 728 cm^{-1}, which can be attributed to COO^-

asymmetric, COO^- symmetric bending vibration, C-H in-plane, and C-H out-of-plane bending vibration, respectively, which are consistent with BTC^- coordinated with Cu^{2+} [90, 105]. All these characteristic peaks overlapped with IR spectra of CMP in Cu-BTC@CMP composites prepared by different procedures, especially in LbL-org and LbL-wtr-org products, which confirm the successful preparation of Cu-BTC@CMP composites.

As shown in Fig. 3-5, spectra of samples prepared by one-pot and two-step procedures present very weak absorbance intensity in characteristic peaks of Cu-BTC, but strong absorbance intensity at around 3300 cm^{-1} and 2800 cm^{-1}, contributed by -OH and C-H in cellulose, especially in the spectrum of sample prepared by one-pot procedure. However, samples prepared by LbL-org and LbL-wtr-org procedures show strong absorbance characteristic peaks of Cu-BTC and very weak absorbance intensity of cellulose, and the absorbance intensity of LbL-wtr-org product is stronger than that of LbL-org product. These results suggest that Cu-BTC crystal deposited on carboxymethylated filter paper can be reinforced by a two-step preparation procedure and further enhanced remarkably by the LbL-wtr-org preparation procedure.

3.3.4 XRD analysis

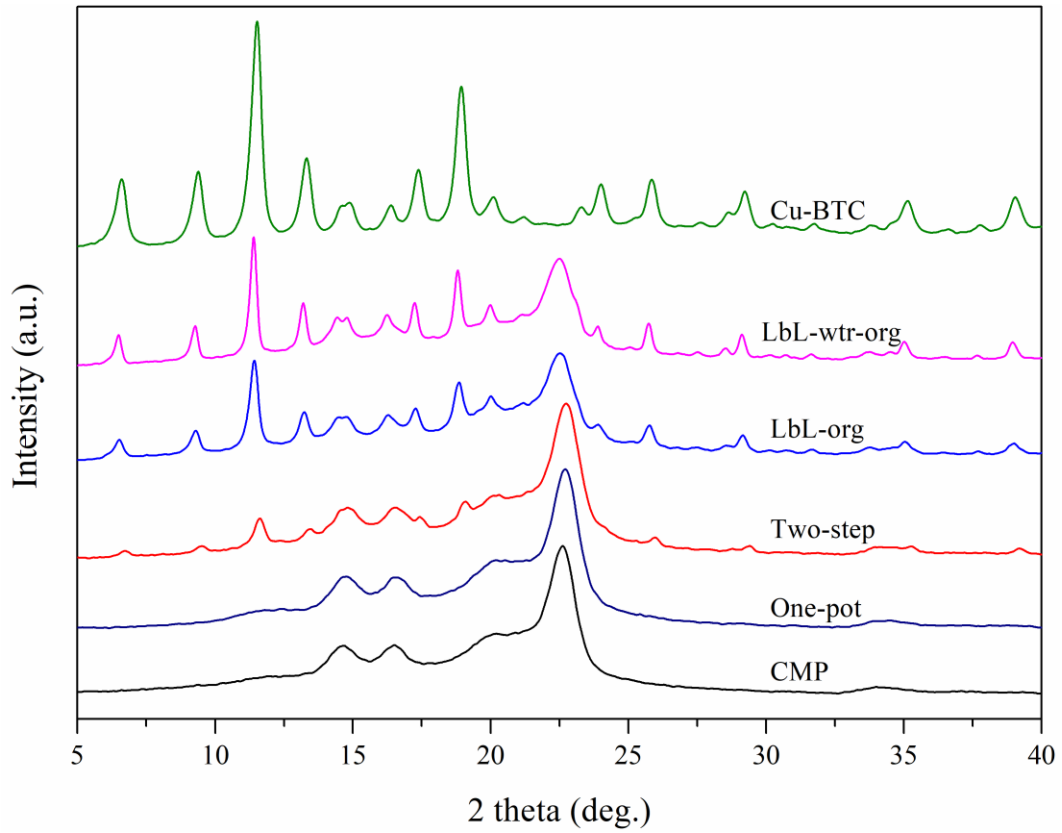

Fig. 3-6 XRD spectra of CMP, Cu-BTC, and Cu-BTC@CMP prepared by different procedures

The XRD patterns of Cu-BTC, CMP, and Cu-BTC@CMP are shown in Fig. 3-6. The CMP sample presents characteristic peaks of cellulose I, as discussed in the carboxymethylation of filter paper part. Characteristic 2θ peaks at 6.6°, 9.4°, 11.5°, 13.3°, 17.4°, 18.9°, 25.7°, and 29.1° are contributed by Cu-BTC crystals [10]. In terms of Cu-BTC@CMP prepared by different procedures (except one-pot procedure), both characteristic peaks of Cu-BTC and CMP can be found, which confirms the growth of

Cu-BTC onto carboxymethylated filter paper.

It was also noticed that the peak intensity of the two-step procedure is more significant compared to the one-pot procedure, which is almost the same as the XRD pattern of CMP. In addition, Cu-BTC@CMP prepared by layer-by-layer method exhibited a remarkable increase of XRD peak intensity, as shown in Fig. 3-6 (LbL-org and LbL-wtr-org), especially in the spectrum of LbL-wtr-org sample, which can be attributed to more Cu-BTC crystals deposited onto the filter paper surface. Therefore, the XRD results are in accordance with the analysis of ATR FT-IR and SEM, which further confirms the presence of Cu-BTC crystals onto CMP surface, LbL-wtr-org procedure will yield higher amount of Cu-BTC onto the paper substrate while reducing the use of chemicals and organic solvents.

3.3.5 Gas adsorption capacity analysis

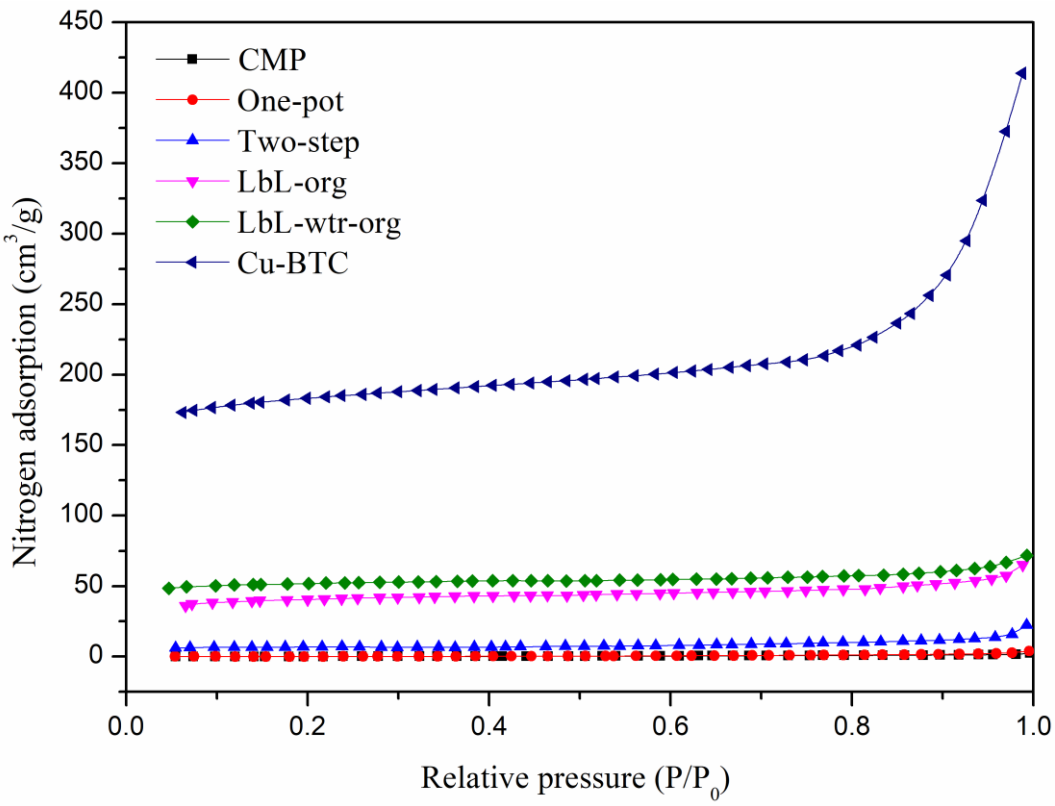

Fig. 3-7 Nitrogen adsorption isotherms of Cu-BTC, CMP, and Cu-BTC@CMP prepared by different procedures

Table 3-3 BET specific surface area, pore volume, and pore diameter of Cu-BTC, CMP, and Cu-BTC@CMP prepared by different procedures

Samples	BET specific surface area (m^2/g)	Pore volume ($\times 10^{-2}$ cm^3/g)	Pore diameter (nm)
Cu-BTC	5.63×10^2	41.0	14.2
LbL-wtr-org	1.59×10^2	3.20	3.93
LbL-org	1.27×10^2	3.80	3.69
Two-step	20.2	2.40	3.38
One-pot	0.290	0.600	3.19
CMP	0.170	0.400	3.37

As a typical porous material, large specific surface area is one of the most significant characteristics of metal-organic frameworks, hence the gas adsorption properties of Cu-BTC@CMP prepared by different procedures, CMP, and Cu-BTC crystal were investigated by N_2 adsorption analysis, as shown in Fig. 3-7 and Table 3-3. The nitrogen adsorption isotherms were tested at 77 K, indicates that both Cu-BTC crystal and Cu-BTC@CMP present a type I adsorption isotherm. The adsorption curves show a significant increase after 0.9 (P/P_0), which was contributed by the capillary condensation effect on samples [119]. The Cu-BTC crystal has the highest adsorption capacity, followed by Cu-BTC@CMP prepared by LbL-wtr-org procedure, LbL-org procedure, two-step procedure, one-pot procedure, and CMP respectively. This order was related to the specific surface area, as shown in Table 3-3. The gas adsorption

capacity increase of Cu-BTC@CMP was contributed by Cu-BTC crystals deposited on the filter paper surface. The Cu-BTC@CMP prepared by LbL-wtr-org procedure has the highest gas adsorption ability compared to other preparation procedures and CMP because of higher deposition of Cu-BTC, as discussed in morphology and deposit ratio part. In terms of pore volume and diameter, due to the large difference of specific surface area contributed by Cu-BTC deposition, both the composites prepared by LbL-wtr-org and LbL-org procedures are greater than those prepared by two-step and one-pot procedures. It should also be noticed that the pore diameter of the composite prepared by LbL-wtr-org is greater than that of LbL-org, but pore volume is smaller, which can be interpreted by the particle size of the Cu-BTC prepared by these two procedures, as shown in Fig. 3-3. The smaller particle size of products prepared by LbL-org procedure resulted in smaller pore diameter and greater pore volume, but a much greater deposit ratio of products prepared by LbL-wtr-org procedure resulted in a higher specific surface area, as shown in Table 3-2 and Table 3-3.

Cu-BTC@CMP prepared by combining two separate steps, layer-by-layer, and water-organic procedure (LbL-wtr-org) has the highest gas adsorption capacity for cellulose-based material as a substrate for metal-organic frameworks deposited while saving chemicals and organic solvents, thereby, having maximum potential in high-valued cellulose products and adsorption fields.

3.3.6 Conclusions

This study systematically investigated the key characteristics and properties of Cu-BTC MOFs deposited onto cellulose filter paper prepared via four different procedures, one-pot, two-step, LbL-org, and LbL-wtr-org. The carboxymethylation treatment of cellulose filter paper would improve carboxylate negative sites for anchoring Cu^{2+} and then enhance the Cu-BTC crystal growth. With the same chemical dosage and reaction time, different deposit ratios were obtained: 1.31% for one-pot, 4.23% for two-step, 31.49% for LbL-org, and 39.38% for LbL-wtr-org, respectively. The Cu-BTC crystals tended to grow in the main solution rather than on the substrate surface and the layer-by-layer method would contribute to a remarkable amount increase of MOFs depositing onto the substrate surface. Compared to the LbL-org procedure, Cu-BTC@CMP prepared by LbL-wtr-org procedure presented a larger particle size, rougher surface, but higher amount of crystals due to the aqueous solution of copper ion precursor. The products prepared by the LbL-wtr-org procedure showed the highest gas adsorption capacity (1.59×10^2 m^2/g of BET specific surface area), which will be an optimal pathway for the preparation of MOFs deposited onto cellulose-based material with the advantages of saving organic solvents and best gas adsorption ability.

Chapter 4

Overall Summary

4.1 Cu-BTC onto lignocellulosic fibers by layer-by-layer method in water

Lignocellulosic fiber material as a substrate was used for immobilizing Cu-BTC metal-organic framework (MOF), the composite was strategically synthesized using trimesic salts as linker sources. The growth of Cu-BTC onto lignocellulosic fiber was conducted in aqueous solution by a layer-by-layer method, and the effect of preparation temperature, time, and number of layers of Cu-BTC deposition was also investigated. The products were characterized by ATR FT-IR, XRD, and SEM. The results showed that the as-prepared Cu-BTC in water was partially hydrolyzed phase of Cu-BTC prepared in organic solvents. Cu-BTC metal-organic frameworks were homogeneously immobilized on carboxymethylated high yield pulp fibers (CHFs). Increasing the growth temperature and time would enhance the deposit of Cu-BTC onto fiber surface slightly, however increasing the growth layers would promote the deposit ratio significantly (from 26.17% to 68.59%, 2 layers to 6 layers). The specific surface area of synthesized Cu-BTC@CHFs had a distinct promotion compared with unmodified fibers, showing a certain gas adsorption capacity.

4.2 Cu-BTC deposited onto cellulosic filter paper via different procedures

Cellulose-based material has been increasingly used as a suitable substrate for depositing metal-organic frameworks (MOFs) in recent years. In this work, MOFs (Cu-BTC) were deposited onto carboxymethylated filter paper (CMP) using four different preparation procedures: one-pot, two-step, layer-by-layer-organic (LbL-org), and layer-by-layer-water-organic (LbL-wtr-org). The products (Cu-BTC@CMP) were comparatively characterized by SEM, ATR FT-IR, XRD, and BET specific surface area analyses. The Cu-BTC crystals were immobilized on the CMP surface, where different deposit ratios (1.31% for one-pot, 4.23% for two-step, 31.49% for LbL-org, and 39.38% for LbL-wtr-org, respectively) were obtained when different preparation procedures were used under the precondition of the same chemical dosage and reaction time. The Cu-BTC crystals were found to grow in the main solution rather than on the substrate surface and the layer-by-layer method would contribute to a remarkable quantity of MOFs depositing onto the substrate surface. The crystals on Cu-BTC@CMP surface prepared by LbL-wtr-org procedure presented a much larger particle size and rougher surface compared to those prepared by the LbL-org procedure due to the aqueous solution of copper precursor. Depositing more Cu-BTC onto CMP surface also endowed the composite prepared by LbL-wtr-org procedure with the highest gas adsorption capacity (1.59×10^2 m^2/g of BET specific surface area). Hence, the LbL-wtr-org procedure will be an optimal pathway for depositing metal-organic frameworks onto cellulose-based materials with the advantages of saving organic solvents and best gas adsorption ability.

Chapter 5

Recommendations for future work

The main objective of this thesis was to develop green synthesis and optimum routes for deposition metal-organic frameworks onto cellulosic materials. As with any work where new insights are studied, there are still lots of opportunities to explore the research of MOFs integrated with cellulosic materials, such as:

(1) Growth of MOFs within the porous cellulosic materials to improvement or functionalization of raw material, for instance, wood or other agricultural residue with tunable removal of lignin.

(2) The mechanical effect and mechanism after MOFs growth on the cellulosic substrates should be investigated, few studies are found in this direction.

(3) Exploring the specific applications of MOFs/Cellulosic materials composites based on different forms of cellulosic materials.

References

1. Yaghi, O M, O'Keeffe M, Ockwig N W, Chae H K, Eddaoudi M, Kim J. Reticular synthesis and the design of new materials. Nature, 2003. 423(6941): p. 705-714.
2. Kitagawa, S, Kitaura R, Noro S. Functional porous coordination polymers. Angewandte Chemie International Edition, 2004. 43(18): p. 2334-2375.
3. Lu, W, Wei Z, Gu Z, Liu T, Park J et al. Tuning the structure and function of metal–organic frameworks via linker design. Chemical Society Reviews, 2014. 43(16): p. 5561-5593.
4. Li, J-R, Kuppler R J, and Zhou H-C. Selective gas adsorption and separation in metal–organic frameworks. Chemical Society Reviews, 2009. 38(5): p. 1477-1504.
5. Suh M P, Park H J, Prasad T K, Lim D-W. Hydrogen storage in metal–organic frameworks. Chemical reviews, 2012. 112(2): p. 782-835.
6. Ma, L, C. Abney C, Lin W. Enantioselective catalysis with homochiral metal–organic frameworks. Chemical Society Reviews, 2009. 38(5): p. 1248-1256.
7. Furukawa, H, Cordova K E, O'Keeffe M, Yaghi O M. The chemistry and applications of metal-organic frameworks. Science, 2013. 341(6149): p. 1230444.
8. Horcajada, P, Gref R, Baati T, Allan P K, Maurin G et al. Metal–organic frameworks in biomedicine. Chemical reviews, 2012. 112(2): p. 1232-1268.
9. Mueller U, Schubert M, Teich F, Puetter H, Schierle-Arndt K, Pastre J. Metal–organic frameworks—prospective industrial applications. Journal of Materials Chemistry, 2006. 16(7): p. 626-636.

10. Tranchemontagne D J, Hunt J R, Yaghi O M. Room temperature synthesis of metal-organic frameworks: MOF-5, MOF-74, MOF-177, MOF-199, and IRMOF-0. Tetrahedron, 2008. 64(36): p. 8553-8557.
11. Butova, V V, Soldatov M A, Guda A A, Lomachenko K A, Lamberti C. Metal-organic frameworks: structure, properties, methods of synthesis and characterization. Russian Chemical Reviews, 2016. 85(3): p. 280.
12. Lee Y R, Kim J, Ahn W S. Synthesis of metal-organic frameworks: A mini review. Korean Journal of Chemical Engineering, 2013. 30(9): p. 1667-1680.
13. Stock N, Biswas S. Synthesis of metal-organic frameworks (MOFs): routes to various MOF topologies, morphologies, and composites. Chemical reviews, 2011. 112(2): p. 933-969.
14. Bang J H. and Suslick K S. Applications of ultrasound to the synthesis of nanostructured materials. Advanced materials, 2010. 22(10): p. 1039-1059.
15. Li H, Eddaoudi M, O'Keeffe M, Yaghi O M. Design and synthesis of an exceptionally stable and highly porous metal-organic framework. nature, 1999. 402(6759): p. 276-279.
16. Eddaoudi M, Kim J, Rosi N, Vodak D, Wachter J, O'Keeffe M, Yaghi O M. Systematic design of pore size and functionality in isoreticular MOFs and their application in methane storage. Science, 2002. 295(5554): p. 469-472.
17. Caddick S. Microwave assisted organic reactions. Tetrahedron, 1995. 51(38): p. 10403-10432.
18. Jhung S H, Lee J H, Yoon J W, Hwang J S, Park S E, Chang J S. Selective

crystallization of CoAPO-34 and VAPO-5 molecular sieves under microwave irradiation in an alkaline or neutral condition. Microporous and mesoporous materials, 2005. 80(1-3): p. 147-152.

19. Kang K K, Park C H, and Ahn W S. Microwave preparation of a titanium-substituted mesoporous molecular sieve. Catalysis letters, 1999. 59(1): p. 45-49.
20. Jhung S H, Chang J S, Hwang Y K, Park S E. Crystal morphology control of AFI type molecular sieves with microwave irradiation. Journal of Materials Chemistry, 2004. 14(2): p. 280-285.
21. Jhung, S H, Lee J, and Chang J S. Microwave synthesis of a nanoporous hybrid material, chromium trimesate. Bulletin of the Korean Chemical Society, 2005. 26(6): p. 880-881.
22. Choi J S, Son W J, Kim J, Ahn W S. Metal–organic framework MOF-5 prepared by microwave heating: Factors to be considered. Microporous and Mesoporous Materials, 2008. 116(1-3): p. 727-731.
23. Martinez Joaristi A, Juan-Alcañiz J, Serra-Crespo P, Kapteijn F, Gascon J. Electrochemical synthesis of some archetypical Zn^{2+}, Cu^{2+}, and Al^{3+} metal organic frameworks. Crystal Growth & Design, 2012. 12(7): p. 3489-3498.
24. Pichon, A, Lazuen-Garay A, and James S L. Solvent-free synthesis of a microporous metal–organic framework. CrystEngComm, 2006. 8(3): p. 211-214.
25. Friščić T. New opportunities for materials synthesis using mechanochemistry. Journal of Materials Chemistry, 2010. 20(36): p. 7599-7605.
26. Garay A L, Pichon A, and James S L. Solvent-free synthesis of metal complexes.

Chemical Society Reviews, 2007. 36(6): p. 846-855.

27. Qiu L G, Li Z Q, Wu Y, Wang W, Xu T, Jiang X. Facile synthesis of nanocrystals of a microporous metal–organic framework by an ultrasonic method and selective sensing of organoamines. Chemical communications, 2008(31): p. 3642-3644.
28. Li Z Q, Qiu L G, Xu T, Wu Y, Wang W, Wu Z Y, Jiang X. Ultrasonic synthesis of the microporous metal–organic framework $Cu_3(BTC)_2$ at ambient temperature and pressure: an efficient and environmentally friendly method. Materials Letters, 2009. 63(1): p. 78-80.
29. Kuppler R J, Timmons D J, Fang Q R, Li J R, Makal T A, et al. Potential applications of metal-organic frameworks. Coordination Chemistry Reviews, 2009. 253(23-24): p. 3042-3066.
30. Ma S, Wang X S, Collier C D, Manis E S, Zhou H C. Ultramicroporous Metal− Organic Framework Based on 9, 10-Anthracenedicarboxylate for Selective Gas Adsorption. Inorganic chemistry, 2007. 46(21): p. 8499-8501.
31. Couck S, Denayer J F, Baron G V, Rémy T, Gascon J, Kapteijn F. An amine-functionalized MIL-53 metal− organic framework with large separation power for CO_2 and CH_4. Journal of the American Chemical Society, 2009. 131(18): p. 6326-6327.
32. Alaerts L, Séguin E, Poelman H, Thibault-Starzyk F, Jacobs P A, De Vos D E. Probing the Lewis Acidity and Catalytic Activity of the Metal–Organic Framework $[Cu_3(BTC)_2]$(BTC=Benzene-1, 3, 5-tricarboxylate). Chemistry-A European Journal, 2006. 12(28): p. 7353-7363.

33. Schröder F, Esken D, Cokoja M, Van Den Berg M W, Lebedev O I, et al. Ruthenium nanoparticles inside porous [Zn_4O (bdc) $_3$] by hydrogenolysis of adsorbed [Ru (cod)(cot)]: a solid-state reference system for surfactant-stabilized ruthenium colloids. Journal of the American Chemical Society, 2008. 130(19): p. 6119-6130.
34. Rosi N L, Eckert J, Eddaoudi M, Vodak D T, Kim J, O'Keeffe M, Yaghi O M. Hydrogen storage in microporous metal-organic frameworks. Science, 2003. 300(5622): p. 1127-1129.
35. Zhao D, Yuan D, and Zhou H C. The current status of hydrogen storage in metal–organic frameworks. Energy & Environmental Science, 2008. 1(2): p. 222-235.
36. Noro S I, Kitagawa S, Kondo M, Seki K. A new, methane adsorbent, porous coordination polymer [{$CuSiF_6$(4,4′-bipyridine)$_2$}n]. Angewandte Chemie International Edition, 2000. 39(12): p. 2081-2084.
37. Soppimath K S, Aminabhavi T M, Kulkarni A R, Rudzinski W E. Biodegradable polymeric nanoparticles as drug delivery devices. Journal of controlled release, 2001. 70(1-2): p. 1-20.
38. Horcajada P, Márquez-Alvarez C, Rámila A, Pérez-Pariente J, Vallet-Regí M. Controlled release of Ibuprofen from dealuminated faujasites. Solid State Sciences, 2006. 8(12): p. 1459-1465.
39. Horcajada P, Serre C, Vallet-Regí M, Sebban M, Taulelle F, Férey G. Metal–organic frameworks as efficient materials for drug delivery. Angewandte Chemie International Edition, 2006. 45(36): p. 5974-5978.
40. Loiseau T, Serre C, Huguenard C, Fink G, Taulelle F, Henry M, et al. A rationale

for the large breathing of the porous aluminum terephthalate (MIL-53) upon hydration. Chemistry-A European Journal, 2004. 10(6): p. 1373-1382.

41. Horcajada P, Serre C, Maurin G, Ramsahye N A, Balas F, Vallet-Regi M, et al. Flexible porous metal-organic frameworks for a controlled drug delivery. Journal of the American Chemical Society, 2008. 130(21): p. 6774-6780.
42. Wyszogrodzka G, Marszałek B, Gil B, Dorożyński P. Metal-organic frameworks: mechanisms of antibacterial action and potential applications. Drug Discovery Today, 2016. 21(6): p. 1009-1018.
43. Abbasi A R, Akhbari K, and Morsali A. Dense coating of surface mounted CuBTC metal–organic framework nanostructures on silk fibers, prepared by layer-by-layer method under ultrasound irradiation with antibacterial activity. Ultrasonics sonochemistry, 2012. 19(4): p. 846-852.
44. Aguado S, Quirós J, Canivet J, Farrusseng D, Boltes K, Rosal R. Antimicrobial activity of cobalt imidazolate metal–organic frameworks. Chemosphere, 2014. 113: p. 188-192.
45. Bazer-Bachi D, Assié L, Lecocq V, Harbuzaru B, Falk, V. Towards industrial use of metal-organic framework: impact of shaping on the MOF properties. Powder Technology, 2014. 255: p. 52-59.
46. Ahmed I and Jhung S H. Composites of metal–organic frameworks: preparation and application in adsorption. Materials today, 2014. 17(3): p. 136-146.
47. Liu Y, Ng Z., Khan E A, Jeong H K., Ching C B, Lai Z. Synthesis of continuous MOF-5 membranes on porous α-alumina substrates. Microporous and Mesoporous

Materials, 2009. 118(1): p. 296-301.

48. Huang A, Dou W, and Caro J. Steam-stable zeolitic imidazolate framework ZIF-90 membrane with hydrogen selectivity through covalent functionalization. Journal of the American Chemical Society, 2010. 132(44): p. 15562-15564.
49. Shekhah O. Layer-by-layer method for the synthesis and growth of surface mounted metal-organic frameworks (SURMOFs). Materials, 2010. 3(2): p. 1302-1315.
50. Shekhah O, Wang H, Kowarik S, Schreiber F, Paulus M, Tolan M, et al. Step-by-step route for the synthesis of metal− organic frameworks. Journal of the American Chemical Society, 2007. 129(49): p. 15118-15119.
51. Li Y S, Bux H, Feldhoff A, Li G L, Yang W S, Caro J. Controllable synthesis of metal–organic frameworks: From MOF nanorods to oriented MOF membranes. Advanced Materials, 2010. 22(30): p. 3322-3326.
52. Gascon J, Aguado S, Kapteijn F. Manufacture of dense coatings of $Cu_3(BTC)_2$ (HKUST-1) on α-alumina. Microporous and Mesoporous Materials, 2008. 113(1-3): p. 132-138.
53. Demessence A, Boissière C, Grosso D, Horcajada P, Serre C, et al. Adsorption properties in high optical quality nanoZIF-8 thin films with tunable thickness. Journal of Materials Chemistry, 2010. 20(36): p. 7676-7681.
54. Usman M, Mendiratta S, Lu K L. Semiconductor metal–organic frameworks: Future low-bandgap materials. Advanced Materials, 2017. 29(6): p. 1605071.
55. Lohe M R, Gedrich K, Freudenberg T, Kockrick E, Dellmann T, Kaskel S. Heating and separation using nanomagnet-functionalized metal–organic frameworks.

Chemical Communications, 2011. 47(11): p. 3075-3077.

56. Hasenknopf B. Polyoxometalates: introduction to a class of inorganic compounds and their biomedical applications. Front. Biosci, 2005. 10(275): p. 10.2741.

57. Maksimchuk N V, Kovalenko K A, Arzumanov S S, Chesalov Y A, Melgunov M S, et al. Hybrid polyoxotungstate/MIL-101 materials: synthesis, characterization, and catalysis of H_2O_2-based alkene epoxidation. Inorganic chemistry, 2010. 49(6): p. 2920-2930.

58. Maksimchuk N V, Kovalenko K A, Fedin V P, Kholdeeva O A. Heterogeneous Selective Oxidation of Alkenes to α, β-Unsaturated Ketones over Coordination Polymer MIL-101. Advanced Synthesis & Catalysis, 2010. 352(17): p. 2943-2948.

59. Kuang X, Wu X, Yu R, Donahue J P, Huang J, Lu C Z. Assembly of a metal–organic framework by sextuple intercatenation of discrete adamantane-like cages. Nature chemistry, 2010. 2(6): p. 461-465.

60. Uemura T, Kitagawa K, Horike S, Kawamura T, Kitagawa S, Mizuno M, Endo K. Radical polymerisation of styrene in porous coordination polymers. Chemical communications, 2005(48): p. 5968-5970.

61. Lee H J, Cho W and Oh M. Advanced fabrication of metal–organic frameworks: template-directed formation of polystyrene@ ZIF-8 core–shell and hollow ZIF-8 microspheres. Chemical Communications, 2012. 48(2): p. 221-223.

62. Furukawa S, Hirai K, Nakagawa K, Takashima Y, Matsuda R, Tsuruoka T, et al. Heterogeneously hybridized porous coordination polymer crystals: fabrication of heterometallic core–shell single crystals with an in-plane rotational epitaxial

relationship. Angewandte Chemie International Edition, 2009. 48(10): p. 1766-1770.

63. Koh K, Wong-Foy A G, Matzger A J. MOF@MOF: microporous core–shell architectures. Chemical Communications, 2009(41): p. 6162-6164.
64. Gurunathan T, Mohanty S, Nayak S K. A review of the recent developments in biocomposites based on natural fibres and their application perspectives. Composites Part A: Applied Science and Manufacturing, 2015. 77: p. 1-25.
65. Updegraff D M. Semimicro determination of cellulose inbiological materials. Analytical biochemistry, 1969. 32(3): p. 420-424.
66. Kim M L, Otal E H, Hinestroza J P. Cellulose meets reticular chemistry: interactions between cellulosic substrates and metal–organic frameworks. Cellulose, 2019. 26(1): p. 123-137.
67. Ozer R, Hinestroza J. One-step growth of isoreticular luminescent metal–organic frameworks on cotton fibers. RSC Advances, 2015. 5(20): p. 15198-15204.
68. Abdelhameed R M, Abdel-Gawad H, Elshahat M, Emam H E. Cu–BTC@cotton composite: design and removal of ethion insecticide from water. RSC Advances, 2016. 6(48): p. 42324-42333.
69. Duan C, Meng X, Liu C, Lu W, Liu J, Dai L, et al. Carbohydrates-rich corncobs supported metal-organic frameworks as versatile biosorbents for dye removal and microbial inactivation. Carbohydrate Polymers, 2019. 222: p. 115042.
70. Dufresne A. Cellulose nanomaterial reinforced polymer nanocomposites. Current Opinion in Colloid & Interface Science, 2017. 29: p. 1-8.

71. Dufresne A. Nanocellulose: a new ageless bionanomaterial. Materials today, 2013. 16(6): p. 220-227.

72. da Silva Pinto M, Sierra-Avila C A, Hinestroza J P. In situ synthesis of a Cu-BTC metal–organic framework (MOF 199) onto cellulosic fibrous substrates: cotton. Cellulose, 2012. 19(5): p. 1771-1779.

73. Rubin H N, Neufeld B H, Reynolds M M. Surface-Anchored Metal–Organic Framework–Cotton Material for Tunable Antibacterial Copper Delivery. ACS applied materials & interfaces, 2018. 10(17): p. 15189-15199.

74. Abdelhameed R M, Rehan M, Emam H E. Figuration of Zr-based MOF@ cotton fabric composite for potential kidney application. Carbohydrate polymers, 2018. 195: p. 460-467.

75. Abdelhameed R M, Kamel O M, Amr A, Rocha J, Silva A M. Antimosquito activity of a titanium–organic framework supported on fabrics. ACS applied materials & interfaces, 2017. 9(27): p. 22112-22120.

76. Wang N, Ouyang X K, Yang L Y, Omer A M. Fabrication of a magnetic cellulose nanocrystal/metal–organic framework composite for removal of Pb (II) from water. ACS Sustainable Chemistry & Engineering, 2017. 5(11): p. 10447-10458.

77. Yang Q, Zhang M, Song S, Yang B. Surface modification of PCC filled cellulose paper by MOF-5 ($Zn_3(BDC)_2$) metal-organic frameworks for use as soft gas adsorption composite materials. Cellulose, 2017. 24(7): p. 3051-3060.

78. Ko J, Kim S K, Yoon Y, Cho K H, Song W, Kim T H, et al. Eco-friendly cellulose based solid electrolyte with high performance and enhanced low humidity

performance by hybridizing with aluminum fumarate MOF. Materials Today Energy, 2018. 9: p. 11-18.

79. Chen G, Koros W J, Jones C W. Hybrid polymer/UiO-66 (Zr) and polymer/NaY fiber sorbents for mercaptan removal from natural gas. ACS applied materials & interfaces, 2016. 8(15): p. 9700-9709.
80. Hou J, Luan Y, Huang X, Gao H, Yang M, Lu Y. Facile synthesis of $Cu_3(BTC)_2$/cellulose acetate mixed matrix membranes and their catalytic applications in continuous flow process. New Journal of Chemistry, 2017. 41(17): p. 9123-9129.
81. Hou X, Zhou H, Zhang J, Cai Y, Huang F, Wei Q. High Adsorption Pearl-Necklace-Like Composite Membrane Based on Metal–Organic Framework for Heavy Metal Ion Removal. Particle & Particle Systems Characterization, 2018. 35(6): p. 1700438.
82. Pimentel B R, Fultz A W, Presnell K V, Lively R P. Synthesis of water-sensitive metal–organic frameworks within fiber sorbent modules. Industrial & Engineering Chemistry Research, 2017. 56(17): p. 5070-5077.
83. Au-Duong A-N, Lee C-K. Flexible metal–organic framework-bacterial cellulose nanocomposite for iodine capture. Crystal Growth & Design, 2018. 18(1): p. 356-363.
84. Ashour R M, Abdel-Magied A F, Wu Q, Olsson R T, Forsberg K. Green Synthesis of Metal-Organic Framework Bacterial Cellulose Nanocomposites for Separation Applications. Polymers, 2020. 12(5): p. 1104.
85. Zhu H, Yang X, Cranston E D, Zhu S. Flexible and Porous Nanocellulose Aerogels

with High Loadings of Metal–Organic-Framework Particles for Separations Applications. Advanced Materials, 2016. 28(35): p. 7652-7657.

86. Matsumoto M, Kitaoka T. Ultraselective Gas Separation by Nanoporous Metal−Organic Frameworks Embedded in Gas-Barrier Nanocellulose Films. Advanced Materials, 2016. 28(9): p. 1765-1769.
87. Lu H, Zhang L, Wang B, Long Y, Zhang M, Ma J, et al. Cellulose-supported magnetic Fe_3O_4-MOF composites for enhanced dye removal application. Cellulose, 2019. 26(8): p. 4909-4920.
88. Küsgens, P, Siegle S, Kaskel S. Crystal Growth of the Metal-Organic Framework $Cu_3(BTC)_2$ on the Surface of Pulp Fibers. Advanced Engineering Materials, 2009. 11(1-2): p. 93-95.
89. Rodríguez H S, Hinestroza J P, Ochoa-Puentes C, Sierra C A, Soto C Y. Antibacterial activity against Escherichia coli of Cu-BTC (MOF-199) metal-organic framework immobilized onto cellulosic fibers. Journal of Applied Polymer Science, 2014. 131(19): p. 40815.
90. Neufeld M J, Harding J L, Reynolds M M. Immobilization of Metal–Organic Framework Copper (II) Benzene-1, 3, 5-tricarboxylate (CuBTC) onto Cotton Fabric as a Nitric Oxide Release Catalyst. ACS applied materials & interfaces, 2015. 7(48): p. 26742-26750.
91. Su Z, Zhang M, Lu Z, Song S, Zhao Y, Hao Y. Functionalization of cellulose fiber by in situ growth of zeolitic imidazolate framework-8 (ZIF-8) nanocrystals for preparing a cellulose-based air filter with gas adsorption ability. Cellulose, 2018.

25(3): p. 1997-2008.

92. Park J, Oh M. Construction of flexible metal–organic framework (MOF) papers through MOF growth on filter paper and their selective dye capture. Nanoscale, 2017. 9(35): p. 12850-12854.
93. Ma S, Zhou H-C. Gas storage in porous metal–organic frameworks for clean energy applications. Chemical Communications, 2010. 46(1): p. 44-53.
94. Britt D, Tranchemontagne D, Yaghi O M. Metal-organic frameworks with high capacity and selectivity for harmful gases. Proceedings of the National Academy of Sciences, 2008. 105(33): p. 11623-11627.
95. DeCoste J B, Peterson G W. Metal–organic frameworks for air purification of toxic chemicals. Chemical reviews, 2014. 114(11): p. 5695-5727.
96. Kreno L E, Leong K, Farha O K, Allendorf M, Van Duyne R P, Hupp J T. Metal-organic framework materials as chemical sensors. Chemical reviews, 2011. 112(2): p. 1105-1125.
97. Farrusseng D, Aguado S, Pinel C. Metal-organic frameworks: opportunities for catalysis. Angewandte Chemie International Edition, 2009. 48(41): p. 7502-7513.
98. Lee J, Farha O K, Roberts J, Scheidt K A, Nguyen S T, Hupp J T. Metal-organic framework materials as catalysts. Chemical Society Reviews, 2009. 38(5): p. 1450-1459.
99. Quirós J, Boltes K, Aguado S, de Villoria R G, Vilatela J J, Rosal R. Antimicrobial metal–organic frameworks incorporated into electrospun fibers. Chemical Engineering Journal, 2015. 262: p. 189-197.

100. Aguado S, Canivet J, Farrusseng D. Facile shaping of an imidazolate-based MOF on ceramic beads for adsorption and catalytic applications. Chemical Communications, 2010. 46(42): p. 7999-8001.

101. Hermes S, Zacher D, Baunemann A, Wöll C, Fischer R A. Selective growth and MOCVD loading of small single crystals of MOF-5 at alumina and silica surfaces modified with organic self-assembled monolayers. Chemistry of materials, 2007. 19(9): p. 2168-2173.

102. Duan, C, Meng J, Wang X, Meng X, Sun X, Xu Y, et al. Synthesis of novel cellulose-based antibacterial composites of Ag nanoparticles@metal-organic frameworks@carboxymethylated fibers. Carbohydrate Polymers, 2018. 193: p. 82-88.

103. Wang C, Qian X, An X. In situ green preparation and antibacterial activity of copper-based metal–organic frameworks/cellulose fibers (HKUST-1/CF) composite. Cellulose, 2015. 22(6): p. 3789-3797.

104. Bunge M A, Ruckart K N, Leavesley S, Peterson G W, Nguyen N, West K N, Glover T G. Modification of fibers with nanostructures using reactive dye chemistry. Industrial & Engineering Chemistry Research, 2015. 54(15): p. 3821-3827.

105. Lange L E, Obendorf S K. Functionalization of cotton fiber by partial etherification and self-assembly of polyoxometalate encapsulated in $Cu_3(BTC)_2$ metal–organic framework. ACS applied materials & interfaces, 2015. 7(7): p. 3974-3980.

106. Zhu L, Zong L, Wu X, Li M, Wang H, You J, Li C. Shapeable Fibrous Aerogels of Metal-Organic-Frameworks Templated with Nanocellulose for Rapid and Large-Capacity Adsorption. ACS nano, 2018. 12(5): p. 4462-4468.

107. Sánchez-Sánchez M, Getachew N, Díaz K, Díaz-García M, Chebude Y, Díaz I. Synthesis of metal–organic frameworks in water at room temperature: salts as linker sources. Green Chemistry, 2015. 17(3): p. 1500-1509.

108. Lu L, Hu C, Zhu Y, Zhang H, Li R, Xing Y. Multi-functional finishing of cotton fabrics by water-based layer-by-layer assembly of metal–organic framework. Cellulose, 2018. 25(7): p. 4223-4238.

109. Tham H M, Japip S, Hua D, Chung T S. Green Layer-by-layer Method for the Preparation of Polyacrylonitrile-Supported Zn(BDC) Membranes. ChemSusChem, 2018. 11(15): p. 2612-2619.

110. Nan J, Dong X, Wang W, Jin W, Xu N. Step-by-step seeding procedure for preparing HKUST-1 membrane on porous α-alumina support. Langmuir, 2011. 27(8): p. 4309-4312.

111. Konduri M K, Kong F, Fatehi P. Production of carboxymethylated lignin and its application as a dispersant. European Polymer Journal, 2015. 70: p. 371-383.

112. Emam H E, El-Bisi M. Merely Ag nanoparticles using different cellulose fibers as removable reductant. Cellulose, 2014. 21(6): p. 4219-4230.

113. Fardim P, Holmbom B. Fast determination of anionic groups in different pulp fibers by methylene blue sorption. TAPPI Membership Directory, 2003. 2(10): p. 28-32.

114. Shoulaifar T K, DeMartini N, Ivaska A, Fardim P, Hupa M. Measuring the concentration of carboxylic acid groups in torrefied spruce wood. Bioresource technology, 2012. 123: p. 338-343.

115. DeCoste J B, Peterson G W, Schindler B J, Killops K L, Browe M A, Mahle J J. The effect of water adsorption on the structure of the carboxylate containing metal–organic frameworks Cu-BTC, Mg-MOF-74, and UiO-66. Journal of Materials Chemistry A, 2013. 1(38): p. 11922-11932.

116. Loera-Serna S, Oliver-Tolentino M A, de Lourdes López-Núñez M, Santana-Cruz A, Guzmán-Vargas A, Cabrera-Sierra R, et al. Electrochemical behavior of [$Cu_3(BTC)_2$] metal–organic framework: the effect of the method of synthesis. Journal of Alloys and Compounds, 2012. 540: p. 113-120.

117. Al-Janabi N, Hill P, Torrente-Murciano L, Garforth A, Gorgojo P, Siperstein F. Mapping the Cu-BTC metal–organic framework (HKUST-1) stability envelope in the presence of water vapour for CO_2 adsorption from flue gases. Chemical Engineering Journal, 2015. 281: p. 669-677.

118. Álvarez J R, Sánchez-González E, Pérez E, Schneider-Revueltas E, Martínez A, et al. Structure stability of HKUST-1 towards water and ethanol and their effect on its CO_2 capture properties. Dalton Transactions, 2017. 46(28): p. 9192-9200.

119. Ma S, Zhang M, Nie J, Yang B, Song S, Lu P. Multifunctional cellulose-based air filters with high loadings of metal–organic frameworks prepared by in situ growth method for gas adsorption and antibacterial applications. Cellulose, 2018. 25(10): p. 5999-6010.

120. Gholampour A, Ozbakkaloglu T. A review of natural fiber composites: properties, modification and processing techniques, characterization, applications. Journal of Materials Science, 2020. 55: p. 829-892.

121. Gui Z, Zhu H, Gillette E, Han X, Rubloff G W, Hu L, Lee S B. Natural cellulose fiber as substrate for supercapacitor. ACS nano, 2013. 7(7): p. 6037-6046.

122. Zhang Y Z, Wang Y, Cheng T, Lai W Y, Pang H, Huang W. Flexible supercapacitors based on paper substrates: a new paradigm for low-cost energy storage. Chemical Society Reviews, 2015. 44(15): p. 5181-5199.

123. He J, Kunitake T, Nakao A. Facile in situ synthesis of noble metal nanoparticles in porous cellulose fibers. Chemistry of Materials, 2003. 15(23): p. 4401-4406.

124. Van Rie J, Thielemans W. Cellulose-gold nanoparticle hybrid materials. Nanoscale, 2017. 9(25): p. 8525-8554.

125. Aarne N, Kontturi E, Laine J. Carboxymethyl cellulose on a fiber substrate: the interactions with cationic polyelectrolytes. Cellulose, 2012. 19(6): p. 2217-2231.

126. Richardson J J, Tardy B L, Guo J, Liang K, Rojas O J, Ejima H. Continuous metal–organic framework biomineralization on cellulose nanocrystals: extrusion of functional composite filaments. ACS Sustainable Chemistry & Engineering, 2019. 7(6): p. 6287-6294.

127. Li Z, Hori N, and Takemura A. Synthesis and characterization of Cu-BTC metal–organic frameworks onto lignocellulosic fibers by layer-by-layer method in aqueous solution. Cellulose, 2020. 27(3): p. 1733-1744.

128. Liu Y, Hu H. X-ray diffraction study of bamboo fibers treated with NaOH. Fibers

and Polymers, 2008. 9(6): p. 735-739.

129. Kim K J, Li Y J, Kreider P B, Chang C H, Wannenmacher N, et al. High-rate synthesis of Cu–BTC metal–organic frameworks. Chemical Communications, 2013. 49(98): p. 11518-11520.

Research Achievement

Journal Articles

(1) Zhiqiang Li, Naruhito Hori, Akio Takemura. Synthesis and characterization of Cu-BTC metal–organic frameworks onto lignocellulosic fibers by layer-by-layer method in aqueous solution[J]. Cellulose, 2020, 27(3): 1733-1744.

(2) Zhiqiang Li, Naruhito Hori, Akio Takemura. A comparative study of depositing Cu-BTC metal–organic framework onto cellulosic filter paper via different procedures[J]. Cellulose, 2020, 27(11): 6537-6547.

Conference

Zhiqiang Li, Naruhito Hori, Akio Takemura. Synthesis and characterization of Cu-BTC metal-organic frameworks onto lignocellulosic fibers by layer-by-layer method in aqueous solution [C] 20th International Symposium on Wood, Fiber and Pulping Chemistry (ISWFPC), 2019, Sep. 09-11th, Tokyo, Japan (Oral)

Acknowledgement

First and foremost, I would like to thank my supervisor, Professor Akio Takemura, who provided me a precious opportunity to pursue a doctorate in the world-famous university, The University of Tokyo. Prof. Takemura gave me considerate instruction and guidance during my PhD, and acted as a role model to me not only academically but also in daily life. As a foreign student, I deeply felt the kindness, patience, toleration, and careful consideration of Prof. Takemura for supporting my research and preparing the thesis. I hereby would like to express my sincere thanks and high respect to Prof. Takemura.

I am grateful to Associate Professor Satoshi Kimura and Assistant Professor Naruhito Hori for their kindly helps of a lot of experiment techniques. Their rich knowledge and patience left a deep impression on me.

I would like to express my thanks to Professor Yuji Matsumoto for his introduction before I came to The University of Tokyo.

I would like to thank Professor Tetsuo Kondo, Associate Professor Tomoya Yokoyama, Associate Professor Tsuguyuki Saito, and Associate Professor Yukiko Enomoto for their contribution to review and improve this thesis.

I am grateful to Dr. Ismawati Palle, Dr. Jingmiao Zhang, Dr. Sikai Chen, and other former and present members of the adhesive science and bio-composites laboratory for their friendly cooperation, good suggestions, and kindly support of my research and life.

Of course, I must say thank you to my parents. My parents have no idea about

scientific research, but they always try their best to support and encourage me to do what I like. Without their constant support, I would never have had the opportunity to start and complete a PhD in Japan.

I am thankful to all the people mentioned above. With their kind support and help, I could have a good time during my doctoral period. Sincerely wish them the best health and success.

Finally, I would like to thank the University of Tokyo Fellowship for financial support of my study life.